CHALMERS

Modeling of thermal effects on interior panels with fabric upholstery

Master's thesis at Volvo Car Corporation

MÅRTEN KARLSSON

Modeling of thermal effects on interior panels with fabric upholstery

MÅRTEN KARLSSON

Department of Applied Mechanics

Division of Material & Computational Mechanics

CHALMERS UNIVERSITY OF TECHNOLOGY

Gothenburg, Sweden 2013

Modeling of thermal effects on interior panels with fabric upholstery
MÅRTEN KARLSSON

Cover:
Figure showing the physical test piece, an ABAQUS model of the textile covered test piece and the von Mises stress results of an elongation test simulation.

Modeling of thermal effects on interior panels with fabric upholstery
Master's thesis at Volvo Car Corporation
MÅRTEN KARLSSON
Department of Applied Mechanics
Division of Material & Computational Mechanics
Chalmers University of Technology

ABSTRACT

To improve the feeling of luxury in the interior of a car many car manufacturers applies a textile to the interior trim panels that covers a large part of the visual surfaces in a car interior. Since the panels are made of plastics they deform quite significantly when they have been subjected to an elevated temperature like it is when a car is left in the sun for a longer period of time. To be able to design an interior panel to minimise these effects there is a need to simulate the deformations using a model for the fabric upholstered panel, a knowledge that has to be developed deeper at Volvo Car Corporation where this thesis were performed.

After finding the actual composite lay-up of the material an attempt was made to get the mechanical properties of the fabric from the manufacturer but the properties needed was something they never tested. Hence the composite were put through a series of experiments to decide the elastic, thermal elongation and creep properties of the whole component. These properties were then transferred to a material model by correlating simulation models replicating the experiments. Finally an A-pillar trim panel of a Volvo car was simulated and compared with an old model that was tuned to fit the results from an older car model.

The composite were found to consist of four layers. One layer with the weave of the textile, one layer of the backing material used in the fabric, one layer consisting of a mix of the backing material and the plastic which is injected behind the fabric in the manufacturing process and finally a layer of the pure plastics. The mixed layer is the layer that connects the fabric to the component.

On the coupon level a good correlation to the experiments were found but at the component level the residual deformations were lower than the previous model and what is expected by experience from previous car models.

The major conclusions of this thesis are that the deformation probably is mostly due to the residual stresses that comes from the injection moulding process. The scatter in the experiments also suggests that there is a significant variation in the mechanical properties over the geometry that also is an effect of the injection process. The variation in mechanical properties could be an effect of the stretch in the fabric which is not uniform over the geometry.

Keywords: back injection, fabric upholstered interior trim panels, thermal loads, textile modeling

Contents

1

Introduction

T<small>HE CALCULATION</small> of thermal effects on interior panels is a crucial part to ensure a high perceived quality in a car. Most of the surfaces that are visual inside of a car fall under the category of interior trim and the panels should not appear to change form if a car is left in the sun for an extended period of time. The panel chosen as a case study in this thesis is the panel covering the A-pillar, the pillar between the front door and the wind shield, see figure 1.1. The reason for choosing this trim part is that it is one of the warmest places and a place where deformations are easy to spot by the costumer hence it is a critical component where simulations are needed.

Figure 1.1: *Location of the A-pillar, the car in this figure is a Volvo V40*

Due to the properties of the polymers used in the interior trim parts in the automotive industries the panel will expand in raised temperatures. Since it is locked in place in certain directions the expansion will introduce stresses in the component. The viscoelasticity is highly dependent on the temperature and at the introduced stress levels, due to the viscoelasticity, the polymers will creep and relax. When the temperature is lowered unwanted residual deformations can occur. Unwanted deformations are deformations that can easily be spotted by the costumer. Some deformations can be hard to see but for instance where the A-pillar meets the windshield there is a black border called

the black-off. If the A-pillar trim is deformed in a non-uniform way it will be easy to spot since there is the reference of the black-off. Also, the trim panel can deform in such a way that it is possible to see behind the panel. This is of course highly unwanted.

1.1 Background

In an isotropic material trim part with a single material the residual deformations after a time of elevated temperature can be modeled with good accuracy. To raise the costumer satisfaction of the interior some, or all panels are covered in a textile and this introduce an anisotropy in the material. In thermal experiments it has been seen that with this textile the residual deformations increase and this is not possible to reproduce in a simulation without accounting for the textile [Oldenbo, 2009].

The panels are made using a technique called back injection moulding where the textile is put in the mould and then the polymer is injected behind the textile. This gives rise to a composite material where the textile is indissolubly attached to a frame which gives the pillar its form and strength [Pötsch *et al.*, 2008]. It also introduces different pretensions through the textile and internal stresses in the component.

Attempts have been made at Volvo Car Corporation to simulate the influence of the textile but the thickness of it and all the other mechanical properties are unknown. Previously it has been simulated as a 0.5 mm thick layer with every parameter, except the thermal expansion, similar to the rest of the component. A correlation with a physical sun simulation proved that a thermal expansion smaller than for the rest of the component gave a residual deformation in the same order and mode as the physical test. A 1 % shrink have also been tried to simulate the pretension that is applied to the textile to prevent it from creasing in heat. No optimization has been done, only one value of each parameter has been tested and it only reproduces the same mode and deformations in the same order. This is a simulation that needs to be more accurate and reliable for new concepts. [Oldenbo, 2009]

1.2 Problem definition

To increase the accuracy in simulation of interior panels with fabric upholstery the material parameters of the textile and the coupling between the textile and the material behind it needs to be examined. This is preferably done using data available in data sheets since the alternative is doing test. These test are not only expensive but also they have to be repeated every time the textile is changed. It would of course be better if the data sheets provide enough information, then the simulation can be done even before the textile is bought. If this is not possible the material parameters have to be found using tests on coupon level and those material parameters can then be used to simulate the whole component.

The objectives of the master's thesis can be summarized as:

> *"Develop a model for calculating deformations in an interior trim part which has a back injected fabric upholstery and has been subjected to thermal loads during a long period of time. The model should be validated through correlation with physical tests."*

To reach this goal a couple of questions, listed below, need to be answered.

1. How does the textile influence the deformation?

2. Is the textile a viscoelastic material?

3. To what detail must the textile be modelled to get a good correlation?

4. How thick is each layer in the polymer/polymer-textile/textile laminate?

5. Does the orientation of the textile matter to the deformations?

6. Which parameter in the textile has the largest effect on the residual deformations?

7. Which is the most significant parameter of the textile influencing the residual deformations?

1.3 Boundaries

Due to limited time and restricted resources some boundaries have to be set on the thesis. The knowledge limitations in combination with the timeframe also set some boundaries. They are also good to keep the thesis on track and not to wander off and doing unnecessary work. Below are the boundaries listed:

1. When a polymer is subjected to sunlight the polymer's mechanical properties will change due to UV-ageing. The relevant properties like the modulus, density and the creep resistance will change depending on what happens in the polymer. The polymer chains can either cross link more or the cross linking can be reduced. Other mechanical properties like tensile strength and elongation at break will also change. [Rabek, 1996]

   This is something that will nor can be investigated in this master thesis, it is not the field of studies of the author nor is it a big issue since the material used is of highly stabilized grade. This means that low levels of degradation due to UV-ageing is expected.

2. The heating of a car will be assumed to be sufficiently slow to not introduce any temperature gradients in the components examined. Hence the components will be modelled such that at any point in time the temperature will be uniform through the component. This is a simplification done in previous simulations at Volvo Car Corporation.

3. The creep model currently used at Volvo Car Corporation is the time hardening form of the power-law model available in ABAQUS:

$$\dot{\epsilon} = A\sigma^b t^n \tag{1.1}$$

   where $\dot{\epsilon}$ is the strain rate, σ is the stress level, A, b, n are material constants and t is the time. The material constants are all dependent on the temperature. For this model there already exist data for the polymer material and to implement a new creep model is too time consuming. Hence a boundary will be that the time hardening creep model will be used. It is though necessary to keep in mind that the accuracy of the model decreases as $n \to 1$.

4. The contacts and other elements in the calculation model for the A-pillar will not be changed. An old calculation model will be used with a different material model on the A-pillar panel. This will also show how the new material model will effect the solution.

2

Theory

In THIS CHAPTER the theories used in the thesis is described briefly. The meaning of this is not to give a complete explanation of the theories used but to give the reader an orientation to be able to follow the discussions done later in the thesis. First some of the manufacturing processes used when producing a fabric upholstered interior trim panel is described. Then the anisotropic thermo-elastic behavior is described and later simplified to orthogonal symmetry, this is the underlying theory that is used in ABAQUS to simulate the textile.

2.1   Manufacturing methods

The process of manufacturing the fabric upholstered trim parts is to use a back injection method that injects the polymer material into a mould where the fabric is already in place. The fabric itself is made up of a backing material and a weave which is laminated together using a process called hot melt lamination.

2.1.1   Hot melt lamination

Hot melt lamination is a technique where two materials are joined into a sandwich using an adhesive that is activated by heat. It is a technique suitable for joining fabric materials since it can be done continually by feeding the fabrics over a series of rollers. The manufacturing involves several steps but simplified it starts with the two materials feed into the machine from two rolls. The adhesive is then applied differently depending on the adhesive type, which can be in the form of a powder or as an adhesive film or web. If it is a powder it is sprayed onto a roller that applies it to one of the materials being joined and if it is a film or web it is fed in between the materials from a third winding system. When the adhesive is in place between the materials it is either heated via IR heaters to activate the adhesive and then pressed together by two rollers or the heat is supplied by the pressure rollers that is usually electrically heated. After a cooling step the joined materials are feed through a winding system rolling the finished product into a suitable size for delivery. [Fung, 2002]

2.1.2 Back injection moulding

Back injection moulding or in-mould lamination is a process where the component is moulded and the fabric is applied in the same manufacturing process. In principle the fabric is put into the mould after which the mould is clamped together. Then the melt is injected behind the fabric and the melt press the fabric against the mould wall and fill the rest of the cavity. The melt partially soak the fabric which after the mould is cooled is laminated to the piece. Depending on the geometry this can give large local stretch in the fabric if the cavity is deep. Therefore some techniques to reduce the stretch of the fabric have been found. First is the injection/compression cyclic moulding which in the clamping state just closes the mould and not apply any compression to it. With a low clamping force the mould is injected a lower pressure to let the fabric fill the mould wall as it can slip at the moulds separation line allowing more fabric to enter the mould where after the mould is clamped with a high force and more melt is injected into the mould at higher pressure. This allows the fabric to fill the mould but with smaller stretch in deep cavities. The fabric can also be preformed before it is inserted into the mould but that adds one more process step before the actual injection moulding.[Kuhlmann, 2001]

2.2 Anisotropic thermoelasticity

The theory of anisotropic thermoelasticity presented below is from [Nowacki, 1986].

Using the Helmholtz free energy $F = U - S\mathcal{T}$ leads to

$$\dot{F} = \dot{U} - S\dot{\mathcal{T}} - \dot{S}\mathcal{T} = \sigma_{ij}\dot{\varepsilon}_{ij} - S\dot{\mathcal{T}} - \dot{S}\mathcal{T} - q_{i,i} + W \tag{2.1}$$

The local statement of the second law of thermodynamics of irreversible processes can be written [Nowacki, 1986, (24) p. 6]

$$\dot{S} + \left(\frac{q_i}{\mathcal{T}}\right)_{,i} - \frac{W}{\mathcal{T}} \geq 0 \Leftrightarrow \dot{S}\mathcal{T} + \mathcal{T}\left(\frac{q_i}{\mathcal{T}}\right)_{,i} \geq W \tag{2.2}$$

Eliminating W in (2.1) and (2.2) gives

$$\dot{S}\mathcal{T} + \mathcal{T}\left(\frac{q_i}{\mathcal{T}}\right)_{,i} \geq \dot{F} - \sigma_{ij}\dot{\varepsilon}_{ij} + S\dot{\mathcal{T}} + \dot{S}\mathcal{T} + q_{i,i} \Leftrightarrow$$

$$\dot{S}\mathcal{T} + \left(\frac{q_{i,i}}{\mathcal{T}} - \frac{q_i\mathcal{T}_{,i}}{\mathcal{T}^2}\right)\mathcal{T} \geq \dot{F} - \sigma_{ij}\dot{\varepsilon}_{ij} + S\dot{\mathcal{T}} + \dot{S}\mathcal{T} + q_{i,i} \Leftrightarrow$$

$$-\left(\dot{F} + S\dot{\mathcal{T}}\right) + \sigma_{ij}\dot{\varepsilon}_{ij} - \frac{q_i\mathcal{T}_{,i}}{\mathcal{T}} \geq 0 \tag{2.3}$$

Assuming that $F \equiv F(\varepsilon_{ij}, \mathcal{T}, \mathcal{T}_{,i})$ we can derivate the free energy with respect to time as

$$\dot{F} = \frac{\partial F}{\partial \varepsilon_{ij}}\dot{\varepsilon}_{ij} + \frac{\partial F}{\partial \mathcal{T}}\dot{\mathcal{T}} + \frac{\partial F}{\partial \mathcal{T}_{,i}}\dot{\mathcal{T}}_{,i} \tag{2.4}$$

Eliminating $\dot{F}$ using (2.4) in (2.3)

$$-\left(\frac{\partial F}{\partial \varepsilon_{ij}}\dot{\varepsilon}_{ij} + \frac{\partial F}{\partial \mathcal{T}}\dot{\mathcal{T}} + \frac{\partial F}{\partial \mathcal{T}_{,i}}\dot{\mathcal{T}}_{,i} + S\dot{\mathcal{T}}\right) + \sigma_{ij}\dot{\varepsilon}_{ij} - \frac{q_i\mathcal{T}_{,i}}{\mathcal{T}} \geq 0 \Rightarrow$$

$$\left(\sigma_{ij} - \frac{\partial F}{\partial \varepsilon_{ij}}\right)\dot{\varepsilon}_{ij} - \left(S + \frac{\partial F}{\partial \mathcal{T}}\right)\dot{\mathcal{T}} - \frac{\partial F}{\partial \mathcal{T}_{,i}}\dot{\mathcal{T}}_{,i} - \frac{q_i \mathcal{T}_{,i}}{\mathcal{T}} \geq 0 \tag{2.5}$$

The inequality (2.5) should hold for all rates $\dot{\varepsilon}_{ij}, \dot{\mathcal{T}}, \dot{\mathcal{T}}_{,i}$ hence the coefficients of the rates must vanish which gives

$$\sigma_{ij} = \frac{\partial F}{\partial \varepsilon_{ij}}, \quad S = -\frac{\partial F}{\partial \mathcal{T}}, \quad \frac{\partial F}{\partial \mathcal{T}_{,i}} = 0 \tag{2.6}$$

Expanding the free energy, $F(\varepsilon_{ij}, \mathcal{T})$ into a Taylor series around the natural state ($\varepsilon_{ij} = 0, \mathcal{T} = T_0$). That is the stress free state at the reference temperature T_0 which usually is set to room temperature.

$$F(\varepsilon_{ij}, \mathcal{T}) = \underbrace{F(0, T_0)}_{\equiv 0} + \underbrace{\frac{\partial F(0, T_0)}{\partial \varepsilon_{ij}}}_{\equiv 0} \varepsilon_{ij} + \underbrace{\frac{F(0, T_0)}{\partial \mathcal{T}}}_{\equiv 0}(\mathcal{T} - T_0) +$$
$$+ \frac{1}{2}\left(\frac{\partial^2 F(0, T_0)}{\partial \varepsilon_{ij} \partial \varepsilon_{kl}}\varepsilon_{ij}\varepsilon_{kl} + 2\frac{\partial^2 F(0, T_0)}{\partial \varepsilon_{ij} \partial \mathcal{T}}\varepsilon_{ij}(\mathcal{T} - T_0) + \frac{\partial^2 F(0, T_0)}{\partial \mathcal{T}^2}(\mathcal{T} - T_0)^2\right) + \dots \tag{2.7}$$

The term $F(0, T_0)$ is the free energy at the natural state which is assumed to be zero. The terms $\frac{\partial F(0, T_0)}{\partial \varepsilon_{ij}}$ and $\frac{F(0, T_0)}{\partial \mathcal{T}}$ is the stress and the entropy at the natural state respectively. These are also assumed to be zero. Then (2.7) becomes

$$F(\varepsilon_{ij}, \mathcal{T}) = \frac{1}{2}c_{ijkl}\varepsilon_{ij}\varepsilon_{kl} - \beta_{ij}\varepsilon_{ij}T - \frac{1}{2}mT^2 + \dots \tag{2.8}$$

where

$$T = \mathcal{T} - T_0, \quad c_{ijkl} = \frac{\partial^2 F(0, T_0)}{\partial \varepsilon_{ij} \partial \varepsilon_{kl}}, \quad \beta_{ij} = -\frac{\partial F(0, T_0)}{\partial \varepsilon_{ij} \partial \mathcal{T}}, \quad m = -\frac{\partial^2 F(0, T_0)}{\partial \mathcal{T}^2}$$

Using the relation $(2.6)_1$ and neglecting the cubic and higher order terms in equation (2.7) gives

$$\sigma_{ij} = \frac{\partial F}{\partial \varepsilon_{ij}} = c_{ijkl}\varepsilon_{kl} - \beta_{ij}T \tag{2.9}$$

which is the law of elasticity, also known as the Duhamel-Neumann relation for an anisotropic body.

There are 81 elastic constants in the fourth order tensor c_{ijkl} ($3^4 = 81$). The symmetry of the stress tensor $\sigma_{ij} = \sigma_{ji}$ gives the left minor symmetry $c_{ijkl} = c_{jikl}$ which reduces the number of independent constants to $\frac{3^2+3}{2} \cdot 3^2 = 6 \cdot 3^2 = 54$. The right minor symmetry $c_{ijkl} = c_{ijlk}$ comes from the symmetry of the strain tensor $\varepsilon_{kl} = \varepsilon_{lk}$ which reduce the number of independent constants to $6 \cdot \frac{3^2+3}{2} = 6 \cdot 6 = 36$. The relation

$$c_{ijkl} = \frac{\partial^2 F(0, T_0)}{\partial \varepsilon_{ij} \partial \varepsilon_{kl}} = \frac{\partial^2 F(0, T_0)}{\partial \varepsilon_{kl} \partial \varepsilon_{ij}} = c_{klij}$$

gives the major symmetry of the tensor of elastic constants $c_{ijkl} = c_{klij}$ which reduces the number of independents further to $\frac{6^2+6}{2} = 21$.

The symetry of σ_{ij} also gives $\beta_{ij} = \beta_{ji}$ hence the second order tensor have 6 independent constant that relates to the elasticity and the thermal properties of the material. Solving equation (2.9) for deformations gives

$$\varepsilon_{kl} = s_{klij}\sigma_{ij} + \alpha_{kl}T \tag{2.10}$$

Where s_{ijkl}, the coefficients of elastic susceptibility, posses minor and major symmetry for the same reasons as c_{ijkl}. α_{ij} which are the coefficients of linear thermal expansion is symmetric $\alpha_{ij} = \alpha_{ji}$ due to the symmetry of ε_{ij} and hence contains 6 independent coefficients. Changing the name of

7

the indices in (2.10) such that kl becomes the summation indices which is the most common way of writing and making use of the symmetry gives

$$\varepsilon_{ij} = s_{ijkl}\sigma_{kl} + \alpha_{ij}T \tag{2.11}$$

The coefficients tensors relations will be describe using Voight-matrix notation. [Nowacki, 1986, pp. 504-505]

2.3 Voight-matrix representation

Since there in the 3-dimensional stress and strain states exist 6 independent stresses and strains the tensors in 2.2 can be represented in the 6-dimensional vector space, this is called a Voight representation. The strain ϵ is in a Voight-matrix form written

$$\epsilon = \begin{bmatrix} \varepsilon_{11} \\ \varepsilon_{22} \\ \varepsilon_{33} \\ \gamma_{23} \\ \gamma_{13} \\ \gamma_{12} \end{bmatrix} \tag{2.12}$$

Where $\gamma_{ij} = 2\varepsilon_{ij}$, $i \neq j$, are called the engineering shear strain components. The reason why it is written like that is because the indices $i \neq j$ appears twice due to the symmetry in equations like (2.9). [Runesson *et al.*, 2006, pp. 12-14]. Let us now consider (2.9) which on matrix form can be written $\boldsymbol{\sigma} = \mathbf{C} : \boldsymbol{\epsilon} - \boldsymbol{\beta}T$ and in a Voight representation as

$$\begin{bmatrix} \sigma_{11} \\ \sigma_{22} \\ \sigma_{33} \\ \sigma_{23} \\ \sigma_{13} \\ \sigma_{12} \end{bmatrix} = \begin{bmatrix} c_{1111} & c_{1122} & \cdots & c_{1112} \\ c_{1122} & & & \\ \cdot & & & \\ \cdot & & & \\ \cdot & & & \\ c_{1112} & \cdot & \cdots & c_{1212} \end{bmatrix} \begin{bmatrix} \varepsilon_{11} \\ \varepsilon_{22} \\ \varepsilon_{33} \\ \gamma_{23} \\ \gamma_{13} \\ \gamma_{12} \end{bmatrix} - \begin{bmatrix} \beta_{11} \\ \beta_{22} \\ \beta_{33} \\ \beta_{23} \\ \beta_{13} \\ \beta_{12} \end{bmatrix} T \tag{2.13}$$

The matrix form of the tensor s_{ijkl} is $\mathbf{S}$ and (2.11) can be written $\boldsymbol{\epsilon} = \mathbf{S} : \boldsymbol{\sigma} + \boldsymbol{\alpha}T$ and in a Voight-matrix form

$$\begin{bmatrix} \varepsilon_{11} \\ \varepsilon_{22} \\ \varepsilon_{33} \\ \gamma_{23} \\ \gamma_{13} \\ \gamma_{12} \end{bmatrix} = \begin{bmatrix} s_{1111} & s_{1122} & s_{1133} & 2s_{1123} & 2s_{1131} & 2s_{1112} \\ s_{1122} & s_{2222} & s_{2233} & 2s_{2223} & 2s_{2231} & 2s_{2212} \\ s_{1133} & s_{2233} & s_{3333} & 2s_{3323} & 2s_{3331} & 2s_{3312} \\ 2s_{1123} & 2s_{2223} & 2s_{3323} & 4s_{2323} & 4s_{2331} & 4s_{2312} \\ 2s_{1131} & 2s_{2231} & 2s_{3331} & 4s_{2331} & 4s_{3131} & 4s_{3112} \\ 2s_{1112} & 2s_{2212} & 2s_{3312} & 4s_{2312} & 4s_{3112} & 4s_{1212} \end{bmatrix} \begin{bmatrix} \sigma_{11} \\ \sigma_{22} \\ \sigma_{33} \\ \sigma_{23} \\ \sigma_{13} \\ \sigma_{12} \end{bmatrix} + \begin{bmatrix} \alpha_{11} \\ \alpha_{22} \\ \alpha_{33} \\ \alpha_{23} \\ \alpha_{13} \\ \alpha_{12} \end{bmatrix} T \tag{2.14}$$

It can easily be recognised that

$$\boldsymbol{\alpha} = \mathbf{C}^{-1}\boldsymbol{\beta} = \mathbf{S}\boldsymbol{\beta} \tag{2.15}$$

Which in Voight-notation is

$$
\begin{bmatrix}
\alpha_{11} \\
\alpha_{22} \\
\alpha_{33} \\
\alpha_{23} \\
\alpha_{13} \\
\alpha_{12}
\end{bmatrix}
=
\begin{bmatrix}
s_{1111} & s_{1122} & s_{1133} & 2s_{1123} & 2s_{1131} & 2s_{1112} \\
s_{1122} & s_{2222} & s_{2233} & 2s_{2223} & 2s_{2231} & 2s_{2212} \\
s_{1133} & s_{2233} & s_{3333} & 2s_{3323} & 2s_{3331} & 2s_{3312} \\
2s_{1123} & 2s_{2223} & 2s_{3323} & 4s_{2323} & 4s_{2331} & 4s_{2312} \\
2s_{1131} & 2s_{2231} & 2s_{3331} & 4s_{2331} & 4s_{3131} & 4s_{3112} \\
2s_{1112} & 2s_{2212} & 2s_{3312} & 4s_{2312} & 4s_{3112} & 4s_{1212}
\end{bmatrix}
\begin{bmatrix}
\beta_{11} \\
\beta_{22} \\
\beta_{33} \\
\beta_{23} \\
\beta_{13} \\
\beta_{12}
\end{bmatrix}
\tag{2.16}
$$

2.4 Orthogonal thermoelasticity

In the textile part of the composite there will exist an orthogonal symmetry. This is because there are two principle directions in the weave.

In [Runesson *et al.*, 2006, p. 193] there are no thermal strains but those equations can be used if we form the mechanical strains. From (2.13) and (2.15) we conclude

$$
\mathbf{C} : \boldsymbol{\alpha} = \boldsymbol{\beta} \Rightarrow \boldsymbol{\sigma} = \mathbf{C} : \boldsymbol{\epsilon} - \boldsymbol{\beta}T = \mathbf{C} : \boldsymbol{\epsilon} - \mathbf{C} : \boldsymbol{\alpha}T = \mathbf{C} : \underbrace{(\boldsymbol{\epsilon} - \boldsymbol{\alpha}T)}_{\boldsymbol{\epsilon}_{mech}}
\tag{2.17}
$$

The two principal directions in the orthogonal textile will be represented by the vectors $\mathbf{a}_1$ and $\mathbf{a}_2$. The third direction is given by $\mathbf{a}_3 = \mathbf{a}_1 \otimes \mathbf{a}_2$. It is also convenient to introduce the structure tensor $\mathbf{A}_i \overset{\text{def}}{=} \mathbf{a}_i \otimes \mathbf{a}_i$. $\mathbf{A}_i$ is a second order symmetric tensor with eigenvectors $\bar{\mathbf{C}}_i$ and eigenvalues A_i. Since these do not change due to a change in coordinate system they are called invariants and A_i is called spectral invariants. The spectral invariants can be formed into basic invariants which are denoted i_1, i_2, i_3 and are defined as [Runesson *et al.*, 2006, pp. 16-19]

$$
i_1 = \sum_{i=1}^{3} A_i, \quad i_2 = \sum_{i=1}^{3} [A_i]^2, \quad i_3 = \sum_{i=1}^{3} [A_i]^3
\tag{2.18}
$$

From now on i_k will denote the kth basic invariant of the second order tensor $\boldsymbol{\epsilon}_{mech}$.

In the case of orthogonal symmetry the free energy F depends only on seven invariants $\{i_1, i_2, i_3\}$ and $\{i_{1(\mathbf{A}_i)}, i_{2(\mathbf{A}_i)}\}$, $i = 1,2$ and $i_{1(\mathbf{A}_i)}, i_{2(\mathbf{A}_i)}$ is defined as [Runesson *et al.*, 2006, p. 193]

$$
i_{1(\mathbf{A}_i)} = \mathbf{A} : \boldsymbol{\epsilon}_{mech} = \mathbf{a}_i \cdot \boldsymbol{\epsilon}_{mech} \cdot \mathbf{a}_i, \quad i_{1(\mathbf{A}_i)} = \mathbf{A} : \boldsymbol{\epsilon}_{mech}^2 = \mathbf{a}_i \cdot \boldsymbol{\epsilon}_{mech}^2 \cdot \mathbf{a}_i
\tag{2.19}
$$

Introducing the orthogonal vectors $\mathbf{a}_1, \mathbf{a}_2, \mathbf{a}_3$ it is possible to choose the integrity basis, that is the set of invariants, such that $F(i_{k(A_i)})$, $k = 1,2$ $i = 1,2,3$. Hence the free energy, F, has six independent invariants. From this choice it is obtained that [Runesson *et al.*, 2006, p. 193 (7.106)]

$$
\boldsymbol{\sigma} = \sum_{i=1}^{3} \left(\frac{\partial F}{\partial i_{1(\mathbf{A}_i)}} \mathbf{A}_i + 2 \frac{\partial F}{\partial i_{2(\mathbf{A}_i)}} \left(\boldsymbol{\epsilon}_{mech} \cdot \mathbf{A}_i \right)^{\text{sym}} \right)
\tag{2.20}
$$

Now, restricting the equation to linear response which impose the restriction

$$\frac{\partial F}{\partial i_{1(\mathbf{A}_i)}} = \sum_{j=1}^{3} \left(\phi_{ij} i_{1(\mathbf{A}_j)} \right), \quad 2\frac{\partial F}{\partial i_{2(\mathbf{A}_i)}} = \phi_{3+i} \tag{2.21}$$

Since $\phi_{ij} = \phi_{ji}$ there is nine independent variables $(\phi_{11}, \phi_{12}, \phi_{13}, \phi_{22}, \phi_{23}, \phi_{33}, \phi_4, \phi_5, \phi_6)$. Equation (2.20) can be written

$$\boldsymbol{\sigma} = \mathbf{C}^e : \boldsymbol{\epsilon}_{mech} \tag{2.22}$$

where $\mathbf{C}^e$ can be written in Voight representation using the coordinate system with $\mathbf{a}_i$ as the basis like [Runesson *et al.*, 2006, p.194 (7.114)]

$$\mathbf{C}^e = \begin{bmatrix} \phi_{11} + \phi_4 & \phi_{12} & \phi_{13} & 0 & 0 & 0 \\ \phi_{12} & \phi_{12} + \phi_5 & \phi_{23} & 0 & 0 & 0 \\ \phi_{13} & \phi_{23} & \phi_{33} + \phi_6 & 0 & 0 & 0 \\ 0 & 0 & 0 & \frac{1}{4}(\phi_5 + \phi_6) & 0 & 0 \\ 0 & 0 & 0 & 0 & \frac{1}{4}(\phi_4 + \phi_6) & 0 \\ 0 & 0 & 0 & 0 & 0 & \frac{1}{4}(\phi_4 + \phi_5) \end{bmatrix} \tag{2.23}$$

The mechanical strain can once again be separated in (2.22) into total strain and thermal strain as

$$\boldsymbol{\sigma} = \mathbf{C}^e : (\boldsymbol{\epsilon} - \boldsymbol{\alpha}T) = \mathbf{C}^e : \boldsymbol{\epsilon} - \mathbf{C}^e : \boldsymbol{\alpha}T = \mathbf{C}^e : \boldsymbol{\epsilon} - \boldsymbol{\beta}^e T \tag{2.24}$$

where of course the constants in $\boldsymbol{\alpha}$ needs to be in the same coordinate system. Solving for $\boldsymbol{\epsilon}$ gives

$$\boldsymbol{\epsilon} = (\mathbf{C}^e)^{-1} : \boldsymbol{\sigma} + \boldsymbol{\alpha}T = \mathbf{S}^e : \boldsymbol{\sigma} + \boldsymbol{\alpha}T \tag{2.25}$$

where

$$\mathbf{S}^e = (\mathbf{C}^e)^{-1} =$$

$$\begin{bmatrix} \frac{\phi_{23}^2 - (\phi_5 + \phi_{12})(\phi_6 + \phi_{33})}{P} & \frac{\phi_{12}(\phi_6 + \phi_{33}) - \phi_{13}\phi_{23}}{P} & \frac{\phi_5\phi_{13} + \phi_{12}(\phi_{13} - \phi_{23})}{P} & 0 & 0 & 0 \\ \frac{\phi_{12}(\phi_6 + \phi_{33}) - \phi_{13}\phi_{23}}{P} & \frac{\phi_{13}^2 - (\phi_4 + \phi_{11})(\phi_6 + \phi_{33})}{P} & \frac{(\phi_4 + \phi_{11})\phi_{23} - \phi_{12}\phi_{13}}{P} & 0 & 0 & 0 \\ \frac{\phi_5\phi_{13} + \phi_{12}(\phi_{13} - \phi_{23})}{P} & \frac{(\phi_4 + \phi_{11})\phi_{23} - \phi_{12}\phi_{13}}{P} & -\frac{\phi_5(\phi_4 + \phi_{11}) + (\phi_4 + \phi_{11} - \phi_{12})\phi_{12}}{P} & 0 & 0 & 0 \\ 0 & 0 & 0 & \frac{4}{\phi_5 + \phi_6} & 0 & 0 \\ 0 & 0 & 0 & 0 & \frac{4}{\phi_4 + \phi_6} & 0 \\ 0 & 0 & 0 & 0 & 0 & \frac{4}{\phi_4 + \phi_5} \end{bmatrix} \tag{2.26}$$

where

$$P = (\phi_6 + \phi_{33})\phi_{12}^2 + \left(\phi_{13}^2 - 2\phi_{23}\phi_{13} - (\phi_4 + \phi_{11})(\phi_6 + \phi_{33})\right)\phi_{12} + \phi_5\phi_{13}^2 + (\phi_4 + \phi_{11})\left(\phi_{23}^2 - \phi_5(\phi_6 + \phi_{33})\right) \tag{2.27}$$

To simplify the writing we introduce new constants that represent the long expressions in $\mathbf{S}^e$ giving

$$\mathbf{S}^e = \begin{bmatrix} s_{1111} & s_{1122} & s_{1133} & 0 & 0 & 0 \\ s_{1122} & s_{2222} & s_{2233} & 0 & 0 & 0 \\ s_{1133} & s_{2233} & s_{3333} & 0 & 0 & 0 \\ 0 & 0 & 0 & 4s_{2323} & 0 & 0 \\ 0 & 0 & 0 & 0 & 4s_{3131} & 0 \\ 0 & 0 & 0 & 0 & 0 & 4s_{1212} \end{bmatrix} \tag{2.28}$$

Assuming that in the weave there are no stresses in the out of plane direction the system can be reduced to plain stress, $\sigma_{33} = \sigma_{13} = \sigma_{23} = 0$ which is commonly used in laminate theory

$$
\begin{bmatrix} \varepsilon_{11} \\ \varepsilon_{22} \\ \varepsilon_{33} \\ \gamma_{23} \\ \gamma_{13} \\ \gamma_{12} \end{bmatrix} = \begin{bmatrix} s_{1111} & s_{1122} & s_{1133} & 0 & 0 & 0 \\ s_{1122} & s_{2222} & s_{2233} & 0 & 0 & 0 \\ s_{1133} & s_{2233} & s_{3333} & 0 & 0 & 0 \\ 0 & 0 & 0 & 4s_{2323} & 0 & 0 \\ 0 & 0 & 0 & 0 & 4s_{3131} & 0 \\ 0 & 0 & 0 & 0 & 0 & 4s_{1212} \end{bmatrix} \begin{bmatrix} \sigma_{11} \\ \sigma_{22} \\ 0 \\ 0 \\ 0 \\ \sigma_{12} \end{bmatrix} + \begin{bmatrix} \alpha_{11} \\ \alpha_{22} \\ \alpha_{33} \\ \alpha_{23} \\ \alpha_{13} \\ \alpha_{12} \end{bmatrix} T \qquad (2.29)
$$

Where the $\mathbf{S}^e$ matrix can be reduced giving

$$
\begin{bmatrix} \varepsilon_{11} \\ \varepsilon_{22} \\ \gamma_{12} \end{bmatrix} = \begin{bmatrix} s_{1111} & s_{1122} & 0 \\ s_{1122} & s_{2222} & 0 \\ 0 & 0 & 4s_{1212} \end{bmatrix} \begin{bmatrix} \sigma_{11} \\ \sigma_{22} \\ \sigma_{12} \end{bmatrix} + \begin{bmatrix} \alpha_{11} \\ \alpha_{22} \\ \alpha_{12} \end{bmatrix} T \qquad (2.30)
$$

and the transversal strains becomes

$$
\begin{bmatrix} \varepsilon_{33} \\ \gamma_{23} \\ \gamma_{13} \end{bmatrix} = \begin{bmatrix} s_{1133} & s_{2233} & 0 \\ 0 & 0 & 0 \\ 0 & 0 & 0 \end{bmatrix} \begin{bmatrix} \sigma_{11} \\ \sigma_{22} \\ \sigma_{12} \end{bmatrix} + \begin{bmatrix} \alpha_{33} \\ \alpha_{23} \\ \alpha_{13} \end{bmatrix} T \qquad (2.31)
$$

The elements in the compliance matrix can be translated to engineering constants as [Agarwal *et al.*, 2006, p. 185]

$$
\begin{aligned}
s_{1111} &= \frac{1}{E_1}, & s_{2222} &= \frac{1}{E_2}, & s_{1122} &= -\frac{\nu_{12}}{E_1} \\
4s_{1212} &= \frac{1}{G_{12}}, & s_{1133} &= -\frac{\nu_{13}}{E_1}, & s_{2233} &= -\frac{\nu_{23}}{E_2}
\end{aligned} \qquad (2.32)
$$

3

Methodology

T<small>O SOLVE</small> the problem formulated in chapter 1 a few main steps needs to be taken. First the relevant properties of all the materials in the laminate have to be acquired. The thickness of each layer has to be examined and a model for the interface between the textile and the frame has to be found. When all these are done a finite element model will be developed for a small test piece where the composite properties will be tuned to later be carried over to a finite element model of the component.

3.1 Material properties

The ideal way, to get the most accurate model, of acquiring all material parameters would be to conduct rigorous tests on the different materials. Tests to find out the Young's modulus, coefficient of linear thermal expansion and the creep properties would ideally have to be conducted, all at several temperatures ranging from $-20°$ C to $\smile 100°$ C.

This would be expensive, time consuming and uncertain since the processing of the material will effect the parameters. The textile is stretched and heated during the injection moulding and how that change the material parameters would not be examined if tests on the textile itself would be conducted. If a method to avoid all these tests and still find a good approximation could be developed it saves money and time not only for this project but also for upcoming projects where the material might not be exactly the same. This means that the preferred method is to take data from data sheets provided by the suppliers and find an acceptable approximation. If these seems to be wrong due to changes of the properties during the manufacturing, or the data does not exist, an optimization with starting point in the data known and some approximation have to be done.

3.1.1 Frame properties

The frame is made of a polymer material called Bayblend® T65. It consists of 65% PC and 35% ABS . The mechanical properties of this material is well known, they have been given by the material supplier and picked from the material database Material Data Center. Calculations using them have also been done with good results[Oldenbo, 2009]. The properties of the Bayblend® T65 is listed in table 3.1. The ABAQUS *CREEP parameters will be explained in section 3.4.

Table 3.1: Material properties of Bayblend® T65

Property	
E-modulus (MPa)	2200 @ 23° C
	1800 @ 60° C
	1600 @ 90° C
Poisson's number	0.4
Density (g/cm^3)	1.13
Coefficiant of thermal expansion $\left(\frac{m}{mK}\right)$	0.80e-4
ABAQUS *CREEP Parameters @ 23° C	A=1.55e-6 B=1.97 n=-0.823
ABAQUS *CREEP Parameters @ 80° C	A=8.33e-6 B=2.16 n=-0.782

3.1.2 Textile properties

The textile consists of a layer of woven polyether fibers and a layer of polyether felt backing. They are laminated together using a technique called hot melt lamination [Borgstena, 2013] which is described in 2.1.1. The felt backing helps the textile stick to the frame. Both the weave and the backing is made of polyether, more specific the polymer polyethersulfone (PES).

The textile is woven using a technique called warp knitting. It does not use a particular warp and weft fiber but the weave can still be different in the length and cross direction. A sketch of the weave can be seen in figure 3.1(a) where depending on the process parameters of the knitting it is not symmetrical in the two main directions. In figure 3.1(b) a close up on the actual weave from an A-pillar of the V40 can be seen.
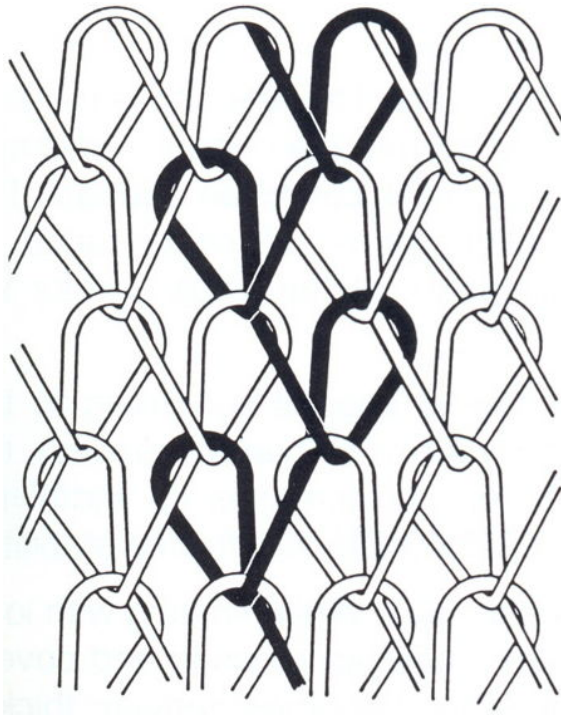
(a) Sketch of the warp knitting technique   (b) Closeup of V40 A-pillar weave
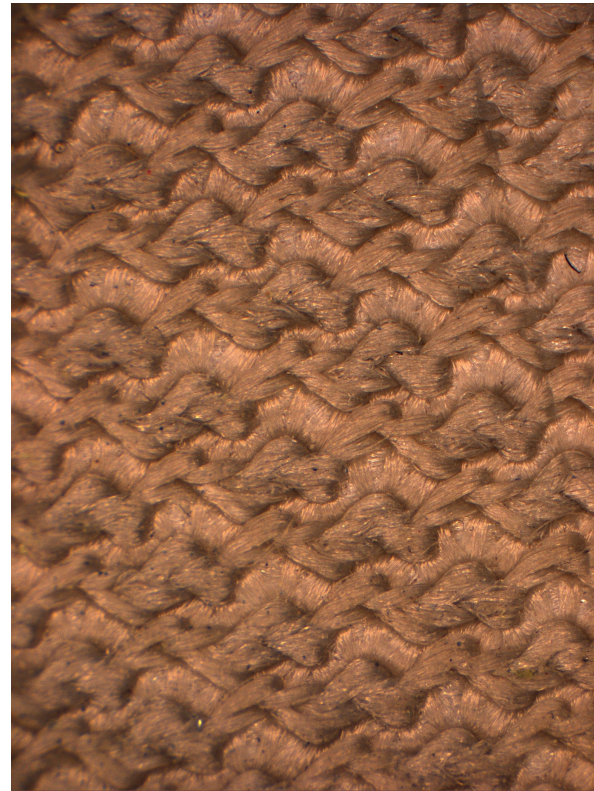
Figure 3.1: *The textile is woven using the warp knitting weaving technique*

The mechanical properties provided by the supplier are few. Except the thickness and weight of the textile the elongation at 100 N is provided in two different measurements, the elongation at break and also the adhesion. If the assumption that the textile is always attached and does not peel of the frame is made the adhesion has no effect on the solution.

Elongation due to mechanical stress

The measurements of the elongation at 100 N are divided into two different properties measured in two different ways. The measurement methods are dictated by Volvo Car Corporation standards where the first standard measure is the elongation at 100 N without pretension. It is done by clamping a textile specimen of 150x50 mm in each end, attaching weights exerting 100 N on the specimen and then measuring the elongation with a ruler.[Volvo Corporate Standard, 1994a]

The second way of measuring includes a pretension of 5 N and a rate-controlled elongation until break. The elongation at 100 N is recorded during the test. The speed of the elongation is set to 100 mm/min, the distance between the clamps are 200 mm and the specimen is 50 mm wide. [Volvo Corporate Standard, 1994b]

The second way of measuring also provides the elongation at break. Both measurements are done at least five times in each of the length and the cross direction. Hence there are two values presented for each measurement, the mean value of the different test results for different samples, in the length and in the cross direction. There are two colours of this textile and the pigment added to the colour

Charcoal alters the mechanical properties. The main work in this thesis will be done on the blonde textile. The elongations are given in two directions and for two different colours as can be seen in table 3.2. The weight and thickness can be seen in the same table.

Table 3.2: Mechanical data of textile for the two different colors. Data taken from data sheet provided by manufacturer [Borgstena, 2013], [Borgstena, 2012]

Property	Zeus Blond PL		Zeus Charcoal Solid PL	
	Length	Cross	Length	Cross
Elongation at 100 N (%)	≥ 13	≥ 13	≥ 11	≥ 11
Elongation at 100 N (%), 5 N pretention	≥ 10	≥ 10	≥ 8	≥ 10
Elongation at break (%)	≥ 60	≥ 60	≥ 60	≥ 60
Weight (g/m^2)	280 ± 30		≥ 300	
Thickness (mm)	1.3 ± 0.3		1.5 ± 0.3	

Assume that the textile deforms linearly elastic from $\varepsilon = 0$ to when the fibers in the direction of elongation are straight and then again linearly elastic with a different modulus, also assume that the fibres in the direction of elongation are straight at the pretension 5 N. The different points on the stress-strain curve will be named:

- ε_0, σ_0 -Initial state when stress and strain is zero
- ε_1, σ_1 -Strain and stress at the pretension state when the force applied is 5N
- ε_2, σ_2 -Strain and stress at the 100N load without pretension
- ε_3, σ_3 -Strain and stress at the 100N load with 5N pretension, hence 105N.

If the textile is modelled as a homogenous body the stress can be calculated as

$$\sigma = \frac{F}{A} = \frac{F}{wd} \tag{3.1}$$

where w is the width and d is the thickness, A is hence the cross-section area of a test specimen. Now, the known things about the stress-strain curve are the point $\{\varepsilon_2, \sigma_2\}$ and the slope of the curve from 5 N to 105 N. The assumption of the piecewise linear curve done earlier now gives the upper part of the stress-strain curve, that is for $\varepsilon > \varepsilon_1$ as

$$\sigma = E_2(\varepsilon - \varepsilon_1) + \sigma_1 \tag{3.2}$$

where the stress σ_1 is known from equation (3.1) using $F = 5$ N. The slope or modulus of the linearly elastic deformation after the fabric is straight, E_2 (see figure 3.2) can be calculated from

$$E_2 = \frac{\sigma_3 - \sigma_1}{\varepsilon_3 - \varepsilon_1} \tag{3.3}$$

where $\sigma_3 - \sigma_1$ is gotten from $105 - 5 = 100$ N put into equation (3.1). ε_1 and ε_3 is unknown but the relation $\varepsilon_3 - \varepsilon_1$, which is the elongation at 100 N with 5 N pretension, is known from table 3.2.

Now since the slope, E_2 and one point on the curve $\{\varepsilon_2, \sigma_2\}$ is known the strain ε_1 can be calculated using (3.2) at the known point

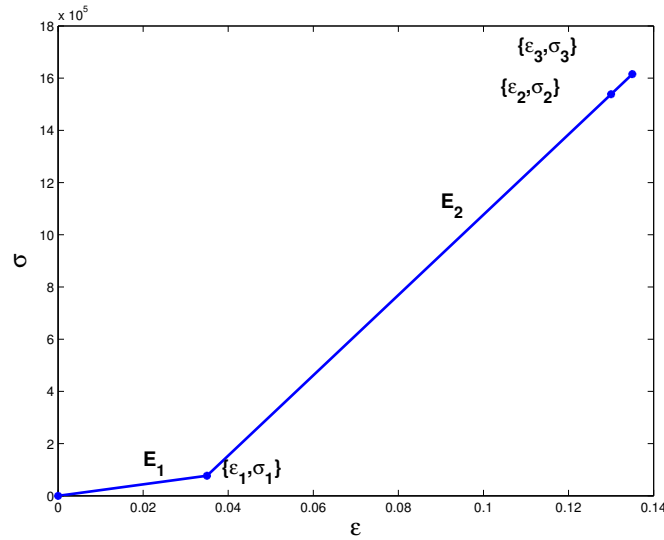$$\sigma_2 = E_2(\varepsilon_2 - \varepsilon_1) + \sigma_1 \Rightarrow$$

Figure 3.2: *Stress-Strain curve for the blond textile in the length direction*

$$\varepsilon_1 = \varepsilon_2 - \frac{\sigma_2 - \sigma_1}{E_2} \tag{3.4}$$

and ε_3 is

$$\varepsilon_3 = \varepsilon_1 + (\text{Elongation at 100 N, 5 N pretension, (table 3.2)}) \tag{3.5}$$

With ε_1 known the modulus of the lower curve can also be calculated as

$$E_1 = \frac{\sigma_1}{\varepsilon_1} \tag{3.6}$$

The resulting curve and the points can be seen in figure 3.2.

This of course only gives the elasticity of the textile in two normal directions at one temperature and as described in section 2.4 there are still several properties needed that the manufacturer can't give. These were found using tests on a coupon level on the complete composite.

Elongation due to thermal stress

The thermal effects on the textile were not given by the textile supplier, hence some tests needed to be performed to get an accurate result. These test where performed on the composite since the textile may change it properties during the injection moulding process. The test procedure will be explained further on in section 3.3.2.

3.2   Composite properties

When the frame material is injected behind the textile it forms a composite with it. As can be seen in figure 3.3 the composite consists of four layers, numbered from the textile side hence from the outside of the component and in they are:

1. The weave is the part of the textile that is woven using the warp knitting technique not including the backing. The properties of it is unknown since the material properties described in section 3.1.2 is for the whole textile.

2. The backing material is made of the same material as the weave but woven in a much looser manner, a different technique and thinner fibers.

3. The mixture between the backing material and the frame material. The mixture can be melted together or the frame material can have wet the fibers in the backing forming a fibre composite where the backing is the fibre and the frame material is the matrix. The typical temperature of the frame material Bayblend® T65 when it is injected into the mold is 240-280° C [Bayer MaterialScience, 2013] and the glass transition temperature of the backing material is $\smile$ 225° C [Klason *et al.*, 2005, p. 130]. Hence the backing and the frame material should melt together but the temperature of the melt decreases as it travels through the mold and the temperature when it mix with the backing material is rather hard to predict.

4. The properties of the frame material, Bayblend® T65 , is known since earlier simulations and correlations at VCC according to 3.1.1.

(a) Cross section

0.1 mm
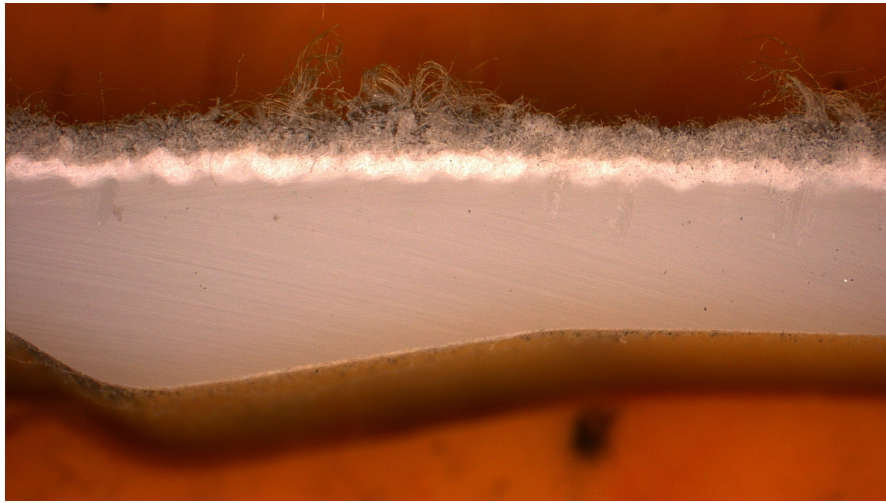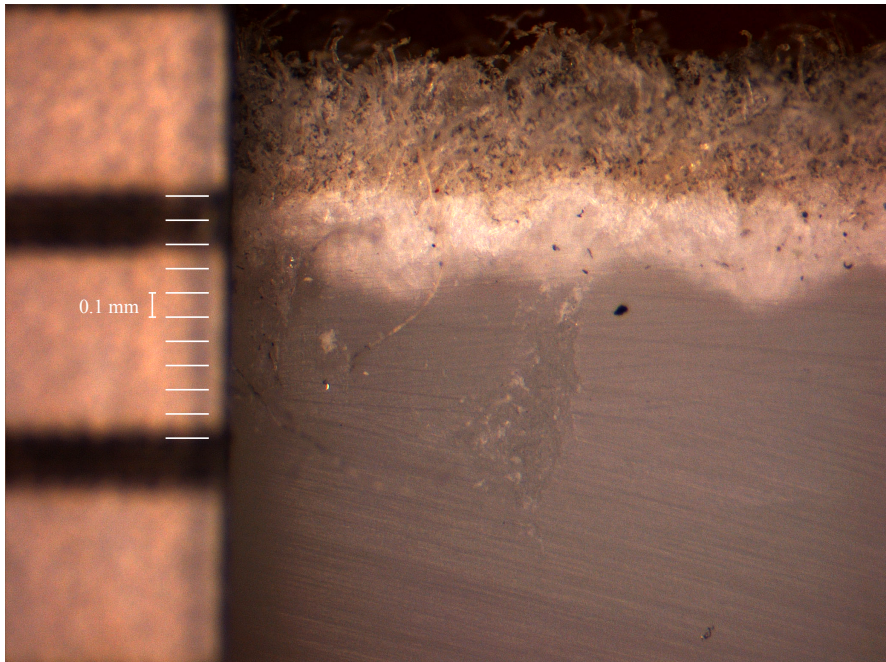
(b) Cross section zoom in. The grading on the ruler is 1 mm

Figure 3.3: *Cross section of the A-pillar of V40. The composite consists of four layers, from textile-side and inwards; 1. Weave, 2. Pure backing, 3. Mixture of backing and frame material, 4. Frame material*

The pictures in figure 3.3 where taken using a microscope. The cross-section was taken from an A-pillar trim panel. The location of the cross-section can be seen in figure 3.6.

The markings that goes from left to right,that can be seen in figure 3.3, are markings from grinding the surface. The grinding were done because the saw that was used to cut the cross-section out of the A-pillar left quite a bad surface that needed to be refined. Hence the markings in the frame material do not prove any material direction in that layer.

The wavy pattern of layer 2 and 3 is probably due to the fibers in layer 1, the weave. The influence of the pattern is assumed to be small compared to the other simplifications done. The A-pillar is usually modelled using shell elements, which will be discussed in section 3.4, with a uniform thickness hence

for instance the reinforcement in the frame material seen to the left in figure 3.3(a) is not modelled. Seen to its thickness it probably has a lot bigger influence on the solution than the wavy pattern of layer 2 and 3.

This will give a good starting point in finding the correct values since the back injection process might have changed the properties even more.

In figure 3.3(b) a ruler was put into the picture for a reference of the scale of the cross-section. The ruler was graded in 1 mm steps and the white marks that where edited into the picture are distanced 0.1 mm apart. The figure 3.3(b) is not good enough to estimate the thickness of the weave since the process of first cutting and then grinding the surface has made the fibers in the weave untwine and it looks thicker than it actually is. This effect can be seen quite easily in figure 3.4. Figure 3.3(b) though gives an indication that the thickness in table 3.2 of 1.3 mm is not the right value when the textile has been processed. One reason for that is that the textile is preformed before it is put in the mold. This stretches the fabric and makes it thinner. Because the fabric's thickness is changed but material is not taken away the elastic modulus must be updated to the new thickness. Hence if the assumption is made that a force will give the same elongation regardless of the thickness the updated Young's modulus becomes, starting from Hook's law,

$$\sigma_{t_1} = E_{t_1}\varepsilon \Rightarrow \frac{F}{wd_{t_1}} = E_{t_1}\varepsilon \Rightarrow \frac{F}{wd_{t_1}E_{t_1}} = \frac{F}{wd_{t_2}E_{t_2}} \Rightarrow \frac{1}{d_{t_1}E_{t_1}} = \frac{1}{d_{t_2}E_{t_2}} \Rightarrow$$

$$E_{t_2} = E_{t_1}\frac{d_{t_1}}{d_{t_2}} \tag{3.7}$$

Figure 3.3(b) also gives the ability to estimate the thickness of the layers 2 and 3. The thickness of the frame material varies over the component and will be simulated, like in previous simulations done at Volvo Car Corporation as uniform using a mean value.
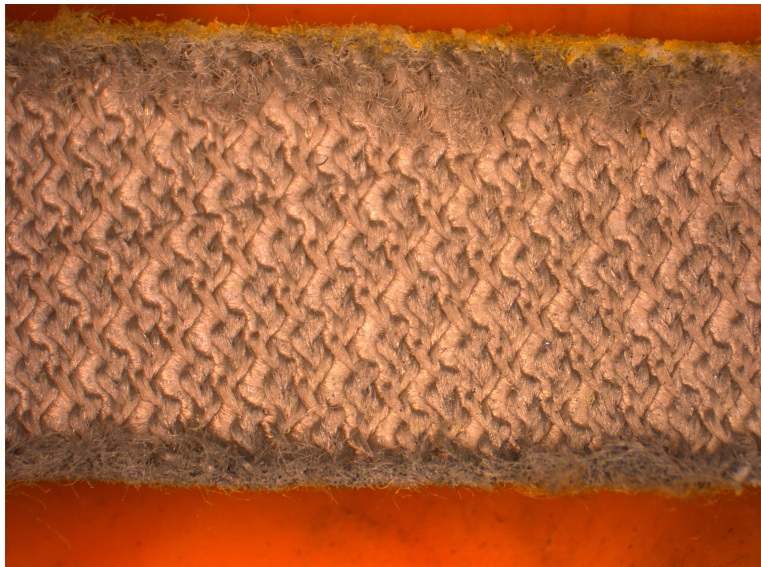

Figure 3.4: *The fibers of the weave have untwined due to the cutting and the grinding. The surface upwards in the figure is only cut with a saw while the lower also is grinded. It is the lower surface that is examined in figure 3.3.*
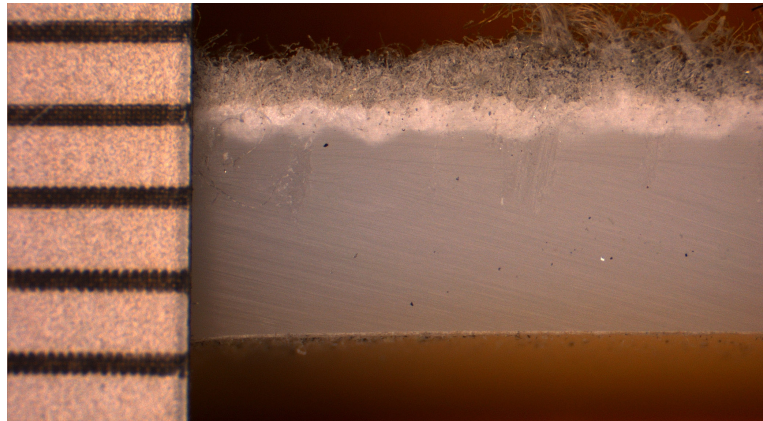
Figure 3.5: *Whole cross-section with a ruler where the black marks are spaced 1 mm apart.*

Figure 3.6: *Location on the A-pillar of the cross-section examined in a microscope*

3.3 Coupon experiments

To find the different parameters of the composite a couple of mechanical tests where conducted. If a creep test where to be conducted at several temperatures all the unknown parameters, the elastic modulus, the thermal elongation and the creep of the textile, would be in play but if several different kinds of tests where conducted the material characteristics can be built up step by step. First a test of the elastic modulus where conducted at room temperature during a short period of time where only the elastic properties are involved. After that a test of the thermal elongation can be conducted where the elastic properties and the thermal elongation is in play and lastly a test on how much the material elongates over time can be conducted at several temperatures where all the parameters plays a role in the outcome.

All the test samples where "dog bone"-shaped standard specimens, se figure 3.7, taken from a B-pillar trim panel. The total thickness of the specimens were 3.4 mm. The reason for taking the B-pillar panel was that there are no flat surfaces sufficiently large on the A-pillar panel and the B-pillar panel has the same materials as the A-pillar. Several of these where taken from three different panels. Though only one material direction could be accomplished and that was where the textile had a 40° angle from the specimens main direction. The shape, size and the textile direction can be seen in

figure 3.7.

Figure 3.7: *Drawing of the test specimen used, the dashed lines indicates the weave principle direction. Drawing from [Volvo Corporate Standard, 2005] with textile direction drawn by the author.*
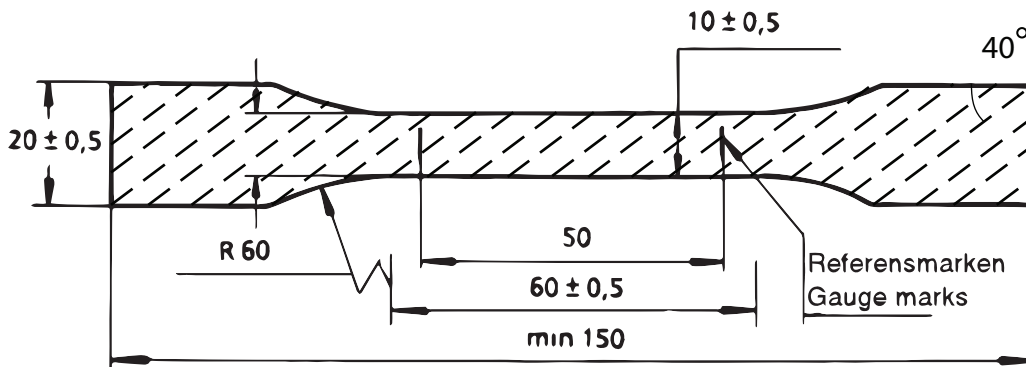
3.3.1 Elasticity experiment

To test the tensile modulus of the whole composite a Zwick tensile tester where used. It measures the force and the elongation when it pulls at a steady rate until the material breaks. When the thickness and width of the material is entered the machine calculates a engineering stress-engineering strain diagram. The elastic modulus is calculated as a mean of the stress over the strain between the strains 0.05 % and 0.25 %. The rate was 1 mm/min in the elastic modulus part and 50 mm/min from the 0.25 % elongation until breakage. The part above the elastic modulus test was not interesting in this thesis since the response of the material is assumed to be linear and the strains sufficiently small.

3.3.2 Thermal experiments

The first method of testing the thermal elongation tried was to take one of the specimen described above, measure the length of it in room temperature and then put it in a climate chamber at 95° C. After two hours the length was measured once again, still in the elevated temperature. One problem with this method was that the test specimen curved towards the textile side. Even if the specimen was pushed down to be flat, no change in the length could be measured with the measurement devices available. The best measurement method that was available where to use a ruler, this because the tools available at Volvo Car Corporation at the time of the tests were not developed for elevated temperatures.

In the thermal elongations test one crucial observation where done. The test specimens curved significantly in elevated temperature. Hence the experiment were conducted once again but this time measuring the height of the middle of the test specimen, first in room temperature and then in 95° C. The specimens rested on a surface with the textile side down.

3.3.3 Creep experiment

To perform a correlation test on the creep parameters the Zwick tension tester were used again but this time with a constant prescribed stress level and the strain measured over time. The stress levels where taken from earlier creep tests made with pure Bayblend® T65. All those previous tests where performed for 1000 h and for two different temperatures, 23° C and 80° C. The lower temperature tests where performed at the stress levels 5, 10 and 15 MPa and the higher temperature at 6, 8 and 10 MPa. Due to time limitations only one stress level from each temperature where chosen and the time where greatly reduced to 24 hours. Even though the time was reduced there would still be a significant creep according to the previous tests done.

3.4 FE-implementation

To simulate the residual deformations both in the full component and the test pieces the FE solver ABAQUS was used. The material was simulated as 3- and 4-node shell elements to save computational resources. If the component would be simulated as continuum 3 dimensional elements they would have to be very small. There would be needed a handful of elements through the thickness and with a thickness of $\sim$ 3 mm the elements would have to be less than one millimeter. Minding the aspect ratio of the elements they would have to be small in the other dimensions too which would give lots of elements to have a high accuracy. The small thickness compared to the other dimensions of the component also justifies the choice of shell elements. This might be questionable in the "dog bone"-shape since the width in the narrower area is only 10 mm and the thickness is about 3-4 mm. Though if 3-dimensional elements would be used here, different elements through the thickness would have to be assigned different materials, which is not a difficult task but it is too different from the way it would be implemented on a real component with shell elements.

The different properties of the different materials will be simulated using the composite module in ABAQUS. In this module the material can be represented in different ways, from isotropic materials to fully anisotropic materials. All the materials except the weave will be simulated as isotropic while the weave will be simulated as orthotropic. This could be done using the elastic type ORTHOTROPIC in ABAQUS where the stiffness matrix $\mathbf{C}^e$ (2.23) have to be given. With the plane stress assumption in the weave the most convenient way is to use the type LAMINA, that is a model for orthotropic materials in plane stress elements. The data needed for this approximation of the weave is the reduced $\mathbf{S}^e$ matrix in (2.30) but written in the engineering constants shown in equation $(2.32)_{1-4}$. The shear modulus G_{13} and G_{23} is also needed to define the transverse shear behavior in the shell elements.[Dassault Systèmes Simulia, 2010].

The ABAQUS *CREEP function is used to give the materials a creep behavior. The law used in this thesis is the time power law, $\dot{\epsilon} = A\sigma^b t^n$ where where $\dot{\epsilon}$ is the strain rate, σ is the stress levels and t is the time. The parameters A, B, n is specific for each material and temperature and is interpolated by ABAQUS to give the whole temperature dependency.

3.5 Optimizing properties

To optimize the parameters and find the unknown ones a FE-model according to the section 3.4 on the geometry of the test pieces where set up. Different load cases where introduce to correlate

against the different experiments. To simulate different parameters and analyse the results a BASH shell script that alters the ABAQUS-input were developed. It reads an input file with the different values of the parameters to test, then writes the first set of data into the ABAQUS-input files. It then sends the calculation to the ABAQUS solver on a computer cluster. When the calculation is finished the script saves the results data and then alters the ABAQUS-input files again and sends a new set of parameters to the cluster. The script can handle any combination of the Young's modulus for the backing, mixing and the different parameters for the weave.

A MATLAB script was also developed to process and present the resulting data from the different runs with the different parameters. That script reads the input data to know which parameters is associated to which results file and then reads all the results. It then plots the correlation against the value of the different parameters. How the correlation and the load cases where set up will be explained below for the different tests.

3.5.1 Elasticity

For the elasticity test a force was applied in the x-direction on one side of the test pice and at the other side the edge nodes where rigid in all directions, see figure 3.8. All nodes where also rigid in the z-direction. The force applied was calculated to give a strain of approximately 0.25 % for a pure Bayblend® T65. To get that a force of F_n in the x-direction are applied in each of the 11 load nodes. To calculate the force F_n the stress that gives 0.25 % strain is first needed. The Bayblend® T65 have a Young's modulus $E_b = 2200$ hence a stress of $\sigma = E_b \cdot 0.0025$ is needed. To get the total force $11F_n = \sigma wt$ the width w and the thickness t is needed. The thickness of the test specimen is 3.4 mm and the width is 10 mm. Some simple algebra now gives

$$F_n = \frac{\sigma wt}{11} = \frac{0.0025 E_b wt}{11} = \frac{0.0025 \cdot 2200 \cdot 3.4 \cdot 10}{11} = 17 \text{ N} \tag{3.8}$$

For the tensile test the ABAQUS solver saved the displacements of two nodes in approximately the same place as the gauge marks in figure 3.7. It also outputted the initial coordinates for that nodes. The MATLAB program then calculated the strain as

$$\varepsilon = \frac{u_2 - u_1}{x_2 - x_1} \tag{3.9}$$

where u is the displacements and x is the initial x-coordinate. To correlate it against the experimental Young's modulus the nominal modulus of the simulation results needs to be calculated. This is done using Hooks law $\sigma = E_e \varepsilon_e$ where σ is known as $0.0025 E_b = 5.5$ N/mm². Hence the simulated mean modulus can be calculated $E_e = \frac{\sigma}{\varepsilon_e} = \frac{5.5}{\varepsilon_e}$ N/mm² and then correlated against the experiment.

The values found using the method described in 3.1.2 where used as a starting point in the correlation process.
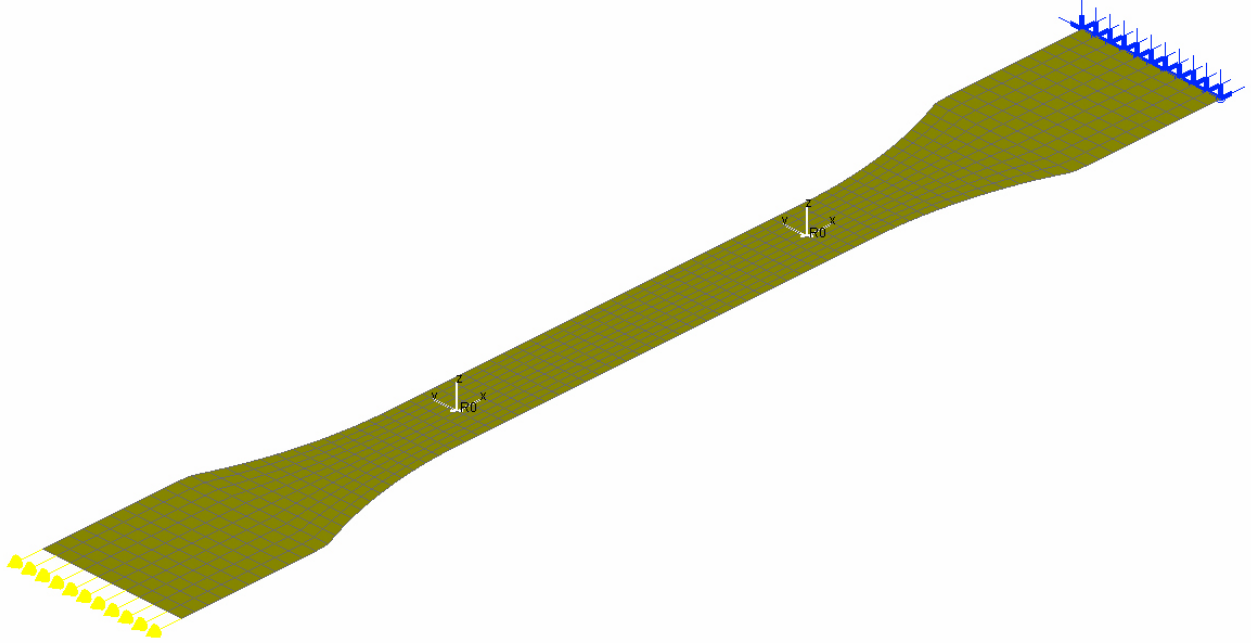
Figure 3.8: *Model of the test specimen showing the load direction the rigid nodes and the gauge nodes*

3.5.2   Thermal elongation

To correlate against the thermal coupon experiments described in 3.3.2 a different load case was introduced to the same model as earlier. The boundary conditions where set to prevent movement in the y,z-direction at the end nodes. One side where also prevented to move in the x direction to prevent rigid body motion. The loads present where the temperature of $95°$ C and the gravitational force.

The ABAQUS-input files where set up to output the displacement of the middle node that then where read by the MATLAB script.

The elastic properties found using the routine described in 3.5.1 where used in the thermal correlating tests but they where only valid for room temperature. The elastic properties thermal dependency is important in this correlation and the assumption is made that the textile materials elastic properties are affected in the same way as the frame material Bayblend® T65 in elevated temperatures. Hence the percentile loss will be the same for the textile and the frame material. This can be described mathematically as

$$\frac{E_{1x}}{E_{2x}} = \frac{E_{1y}}{E_{2y}}$$

where the numerical indices 1 and 2 means different temperatures and x,y is different materials. This can be rearranged to calculate the new elastic property of the textile components which in this case is denoted material x at the temperature 2 using the Bayblend® T65 , y, properties at the same temperatures

$$E_{2x} = E_{1x}\frac{E_{2y}}{E_{1y}} \tag{3.10}$$

3.5.3 Creep

To get the creep properties the same model as the elasticity correlation, see 3.5.1, was used but with a different load. A step of raising the temperature and maintaining an elevated temperature for the same duration as the experiment where implemented in the ABAQUS calculation. The same gauge nodes where used but the value saved for each time increment to get the time history of the displacements. The force to be applied for a given stress level are given by the first step of (3.8).

The MATLAB program calculates the strain again using (3.9) but this time for several instances in time and plots the correlation against the experiments done according to section 3.3.3.

3.6 Component correlation

To test the material model on a component a feasible FE-model for an A-pillar panel assembled in a cut out part of a FE-model of the car body, supplied by Volvo Car Corporation, was used. The A-pillar model though have a concept similar to the V40 A-pillar and a correlation for the old model with a 0.5 mm textile layer with a lower thermal expansion have been made in [Oldenbo, 2009]. In that report the thermal expansion of the textile have been optimized to get a correlation that shows the right mode and order of deformations. This correlation where done for the A-pillar in earlier projects, projects that developed the second generation Volvo S80, that also uses the same concept for the A-pillar.

The simulation where run using all of the combinations that gave a suitable correlation using the method in 3.5.

4

Results

U SING THE METHOD described in chapter 3 the results in this chapter was produced. Since the analytical calculations of the material parameters only served as an initial guess all the results have been found by comparing simulations and experiments and optimizing the material parameters. The concluding simulation of the A-pillar component serves as a comparison to see the differences from the present way of simulating the textile. This chapter also discuss the results as they are presented.

4.1 Coupon level experiments

The results of the coupon tests where in some cases quite scattered. Unfortunately it was not recorded which sample came from which panel and exactly where on that panel they came from. Hence the variation in the results can not be proven to have a relation to where it came from though that might still possibly be the reason for the variation.

4.1.1 Tensile experiment

The five tests in the tensile experiments gave a scattered results. The results data can be seen in table 4.1 and a graphical representation of the stress versus strain is plotted in figure 4.1. The mean Young's modulus, E_{mod} from all five experiments where 2126 N/mm^2 but in the data it can be seen that test number 4 is significantly higher than the other tests. This extreme value is probably due to a measurement error or an abnormality in the material and will hence be excluded giving a mean value of 1815 N/mm^2. This is the value that will be used in the comparisons with the FEM-models.

Table 4.1: Results from tensile experiment

No	E_{mod} [N/mm²]	F_{max} [N/mm²]	dL at F_{max} [%]	F_{break} [N/mm²]	dL at break [%]
1	2700	40.7	2.5	32.8	10.5
2	1360	40	2.8	32.8	9.6
3	1550	40.4	2.8	33.1	18.3
4	3370	42.3	2.4	33.5	7.4
5	1650	40	2.7	33	12.9
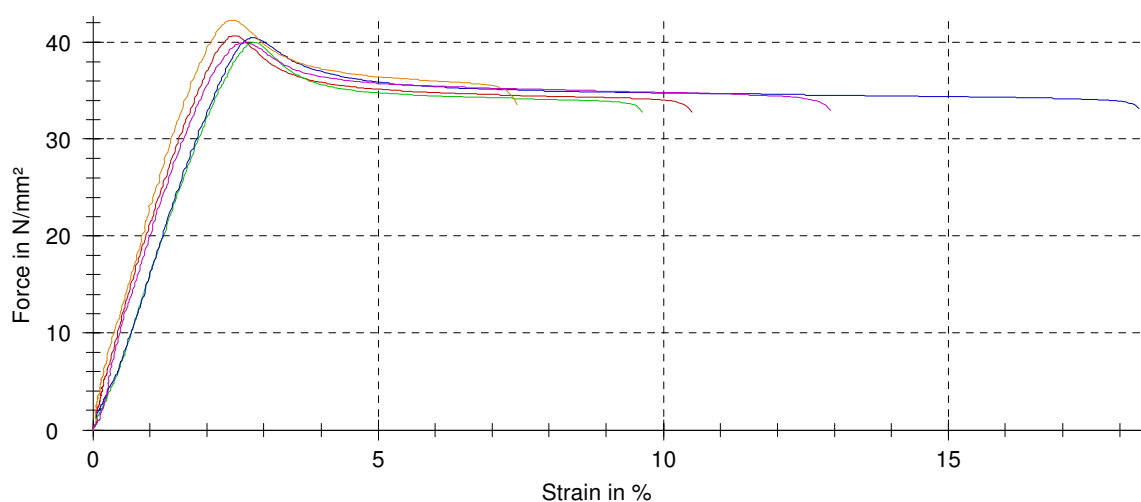
Figure 4.1: *Stress versus strain in tensile experiment*

The variation in the experimental results is of course not desirable in such a small batch of samples. These scattered results could also suggest that the geometry and manufacturing process plays a big role in the tensile strength in the component.

4.1.2   Thermal experiment

The results from the thermal experiments can be seen in table 4.2. Notable is that sample number one have a residual deformation after the test while sample number two don't. It can though be seen that both of them shrinks 0.5 mm from 95° C to room temperature. Hence the thermal effects on the specimens is that they bends such that the middle of the dogbone raises 0.5 mm in the direction of the backing material.

Table 4.2: Results from thermal experiment showing hight in the middle of the specimen before test (h_1), at elevated temperature of 95° C (h_2) and after cool down to room temperature h_3

Sample No	h before test [mm]	h at 95° C [mm]	h at RT after test C [mm]
1	6.5	8.5	8
2	6	6.5	6

The difference between sample 1 and 2 is that one goes back to the original shape after the cool down. Since the samples was taken from different places in a B-pillar trim panel this might suggest that the residual stresses vary significantly over the component. These samples where though taken from places that had the same geometry, as flat as possible, and the residual stresses might very well be worse in other parts of the component.

4.1.3 Creep experiment

The creep experiments recorded the time since start and the elongation in mm and gave 64001 data points for each of the samples. Two samples in 80° C and two in room temperature where tested. The results can be seen in figure 4.2. The initial sharp raise of the elongation is when the test specimen is subjected to the ramp of the initial load of 15 MPa and 10 MPa for the room temperature and 80° C respectively. To make the results comparable the elongation needs to be divided with 50 mm, which is the distance between the gauge marks, to get the strain.

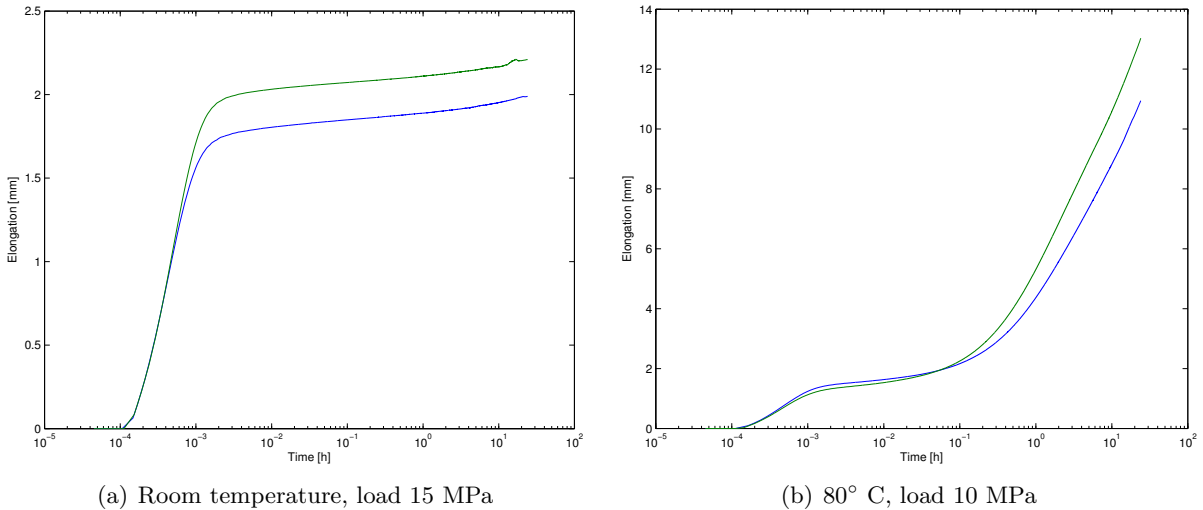(a) Room temperature, load 15 MPa

(b) 80° C, load 10 MPa

Figure 4.2: *Creep experiment results with elongation in mm*

Once again the scatter in the elastic properties, discussed in 4.1.1, can be seen in figure 4.2(a) but the creep seams to be close to the same for the two samples. In 80° C the elastic properties looks to be almost the same but the creep strains is different between the samples.

4.2 Optimization and correlation on coupon level

Using the results presented in section 4.1 the properties of the different materials in the simulations where tuned. Where the properties where totally unknown the starting point was the corresponding property of the Bayblend® T65. Different transversal shear modulus, G_{13} and G_{23}, where tested and where found to play an insignificant role in the coupon test.

4.2.1 Elastic properties

Using the scripts described in section 3.5.1 many different combinations of the elastic properties where investigated. The effect on the solution of Poisson's ratio was first investigated. The Bayblend® T65 have a Poisson's ratio of 0.4, according to table 3.1, hence that and 0.3 was tested for one high and one low elastic modulus for each of the materials and in combination with each other. The input values, the correlation to the nominal elastic modulus of the dogbone and the difference between having all materials Poisson's ratio 0.3 and 0.4 can be seen in table A.1. All possible combinations of the Poisson's ratios, rendering in total 64 results, where also tested but it had the biggest effect when the different materials had the same value. That is, using a fix Young's modulus the biggest difference was unsurprisingly achieved by changing all of the materials Poisson's ratio. These are the results that are compared in table A.1 in appendix A. Since the difference was small between the two Poisson's ratios it was decided to use only one of them.

Using a Poisson's ratio of 0.4 for all the materials several different combinations of Young's modulus were tested. Also the shear modulus of the weave was found to play a significant role in the correlation. With a starting point in the values found from equations derived in 3.1.2, which produce the values in table 4.3, several plots as the one in figure 4.3 where created. Using these kinds of plots several combinations of values for the different materials Young's modulus where found to give a good correlation. Figure 4.4 shows the correlation for different combinations of the Young's modulus and table A.2 gives the correlation and values.
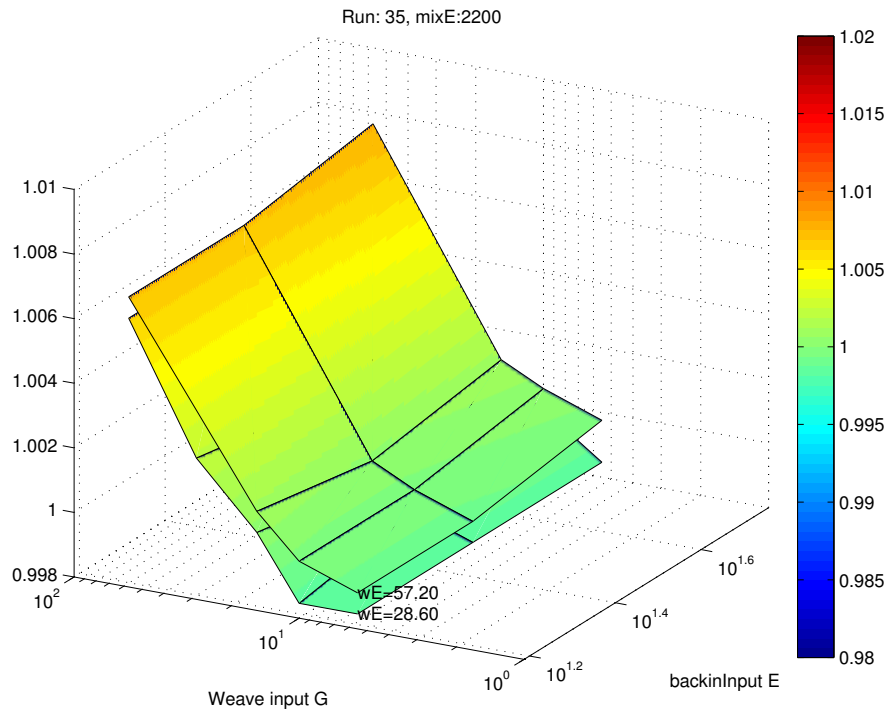
Figure 4.3: *Elastic correlation with a fixed value of the Young's modulus at 2200 N/mm² for the mixture between the backing and the Bayblend® T65. The different layers in the figure represents different elastic modulus in the weave and the x-axis is the in-plane shear modulus. The y-axis shows the elastic modulus of the backing and the z-axis is the correlation to the experimental results. The color also represents the correlation*
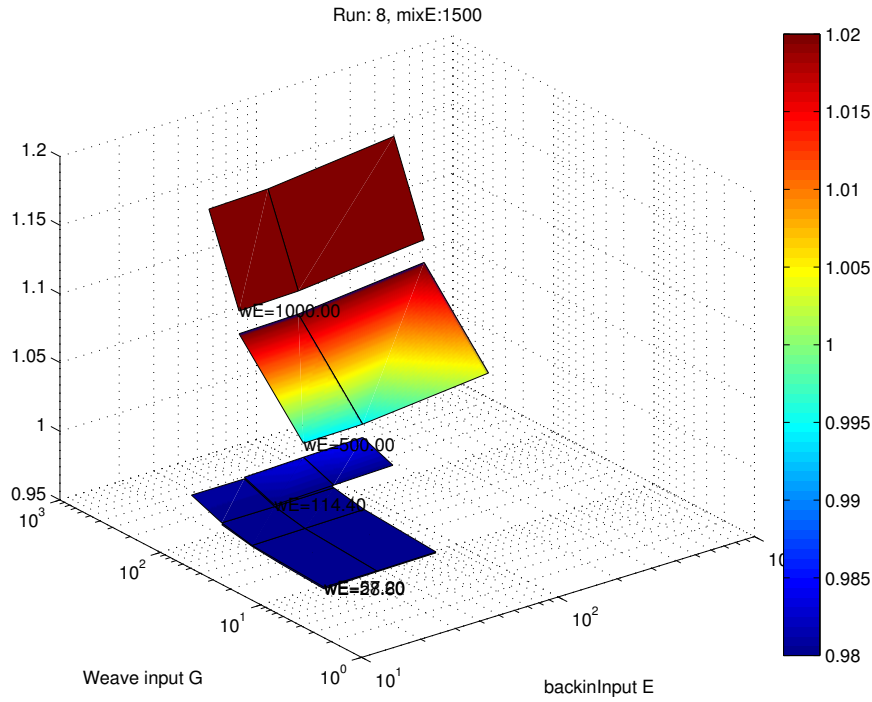
(a) Correlation with the mix modulus at 1500 N/mm^2
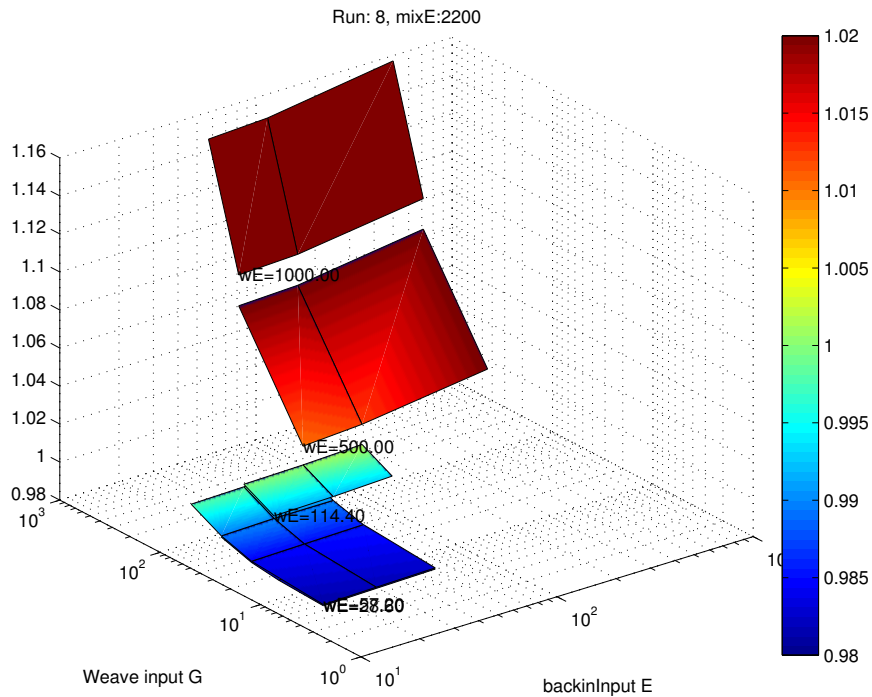
(b) Correlation with the mix modulus at 2200 N/mm^2

Figure 4.4: *Elastic correlation. The different layers in the figure represents different elastic modulus in the weave and the x-axis is the in-plane shear modulus. The y-axis shows the elastic modulus of the backing and the z-axis is the correlation to the experimental results. The color also represents the correlation*

Table 4.3: Young's modulus of the textile calculated using data provided by the manufacturer

Young's modulus	Zeus Blond PL		Zeus Charcoal Solid PL	
	Length	Cross	Length	Cross
E_1 (MPa)	2.2	2.2	2.3	5.1
E_2 (MPa)	15.4	15.4	19.2	15.3

To reduce the time that had to be spent in the coming steps two sets of values where chosen that were deemed reasonable and diverse from each other. These values can be seen in bold in table A.2 and will further on be called set one and set two of elastic properties with elastic set one having $E_{mix} = 1500$ N/mm^2.

4.2.2 Thermal properties

Using the correlated elastic properties from above several thermal expansion coefficients where tested for the different material layers. The starting point was the thermal elongation in the Bayblend® T65 which is 8×10^{-5}. Starting with 1×10^{-5} to 1×10^{-4}, the results in figure 4.5 where produced using the MATLAB script described in 3.5.2.
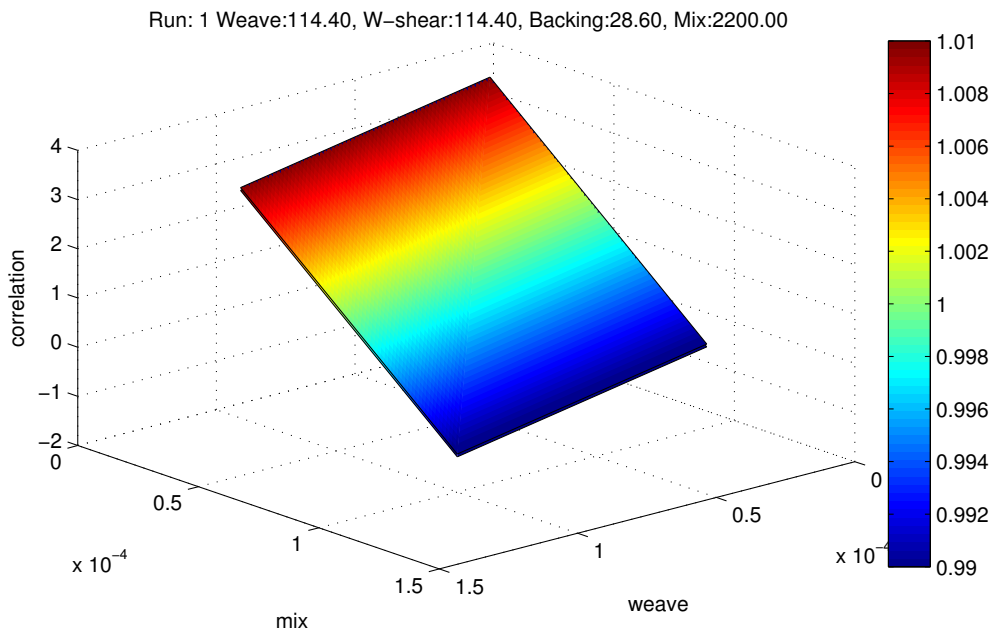
(a) First run using the first set of elastic properties correlating coefficient of thermal elongation.
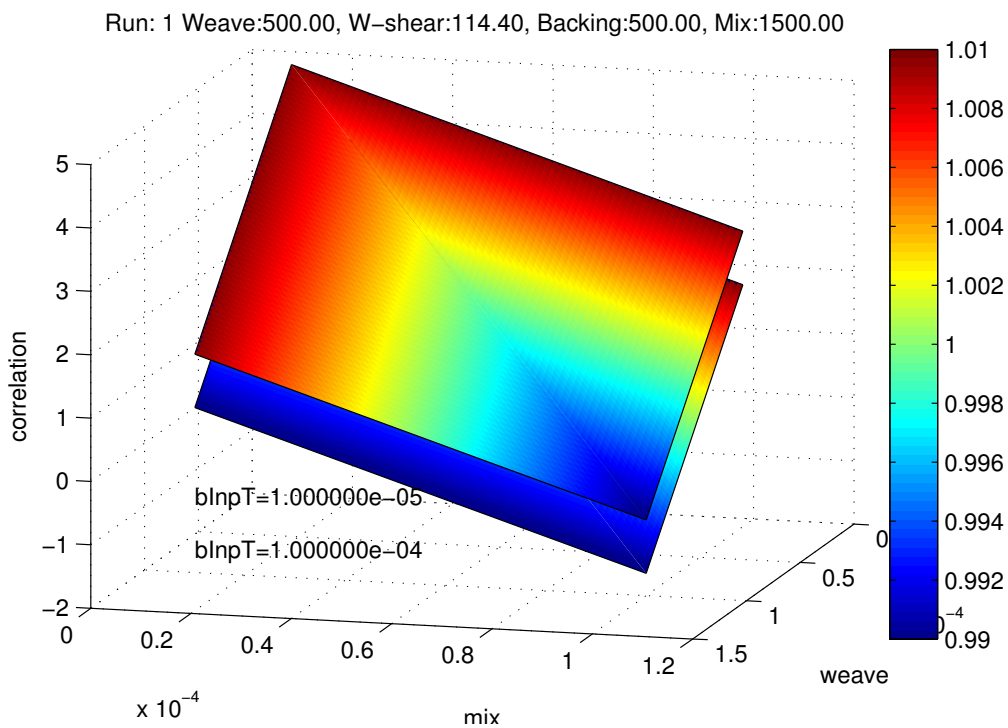
(b) Using the second set of elastic properties correlating coefficient of thermal elongation.

Figure 4.5: *Results from the first run of the thermal correlation, on the x-axis is the coefficient of thermal elongation of the weave and on the y-axis the corresponding for the mixed layer. The layers in the results represents the different coefficients of thermal elongation in the backing material. The z-axis and the color represents the degree of correlation to the physical tests of the material.*

It can be seen in figure 4.5 that the coefficient of thermal elongation for the backing material plays a more significant role in the second set of elastic parameters where the elastic modulus of the backing

material is 500 MPa compared to the first set where the backing has a modulus of 28.6 MPa.

The calculations were then refined around the values where the correlation was good and different values where tested for the different sets of elastic properties.

Since the coefficient of thermal elongation of the backing material was found to have a small impact on the solution the value of the Bayblend® T65 (8×10^{-5}) was used. Using a narrower interval of the parameters to test and a better resolution the correlations in figure 4.6 where produced. From this figure three iterations where done in different areas to catch the fact that different combinations of the coefficient of thermal expansion can provide a sufficient correlation. The resulting values of the coefficients of thermal expansions can be found in table 4.4

The second set of elastic properties, where the coefficient of thermal expansion for the backing played a significant role, was tested for three different values for the coefficients of thermal expansion of the mix. These values represent the interval where a combination of the other parameters within reasonable values can produce a acceptable correlation. Fixing those values the two remaining parameters where iterated into a narrower interval to find a correlation that was sufficiently good. The results can be found in table 4.4 and it can also be seen that for one of the values of the coefficient of thermal expansion of the mix there was two combinations of parameters that gave a good correlation.

Hence after the elastic and thermal correlation there are seven combinations of the elastic and thermal parameters that gives a good correlation.

Table 4.4: Resulting combinations and correlation to experiments for the coefficient of thermal expansion.

Therm set	Elast set	α weave	α backing	α mix	Correlation
1	1	4.4e-05	8e-05	6.1e-05	0.9994
2	1	5.45e-05	8e-05	5.85e-05	0.9996
3	1	5.65e-05	8e-05	5.8e-05	1.0008
4	2	7.75e-05	7e-05	4e-05	0.9996
5	2	6.3e-05	7.6e-05	6e-05	1.0014
6	2	6.95e-05	4.95e-05	6e-05	0.999
7	2	5.75e-05	4.5e-05	8e-05	1.0028
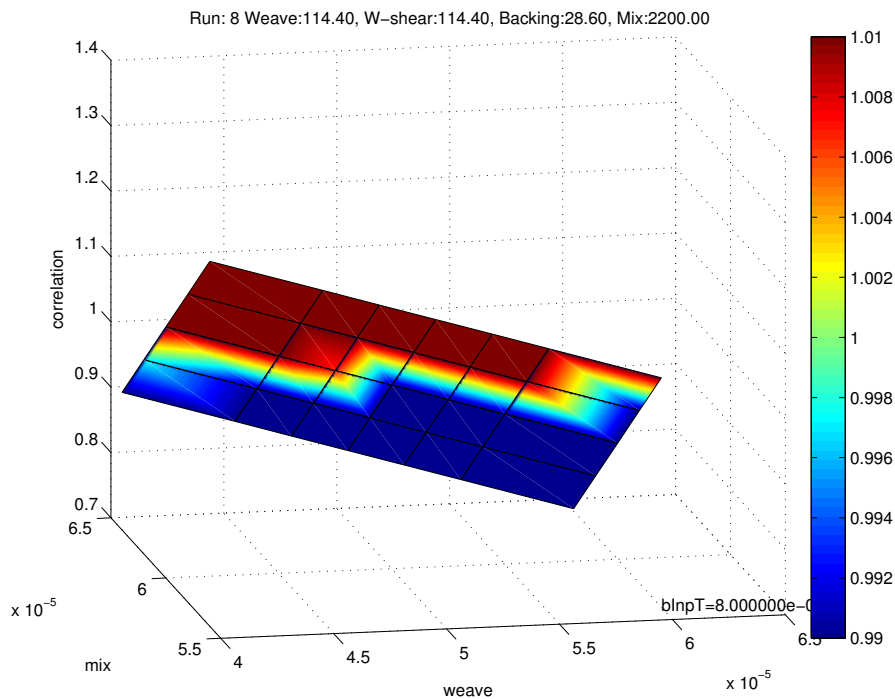
Figure 4.6: *Results from run 8 using only the first set of elastic properties with a greater resolution.*

4.2.3   Creep properties

To be able to correlate the creep values from the simulations and the experiments which both shows the total strain, including both the elastic strain and the creep strains. Therefore a point where the strain developed further on where only due to the creep strains needed to be found. In the simulations that was easy enough because the output only comes from the third step where the load is stable for 24 hours and therefor the strains developing from here on is only due to the creep.

For the creep experiments it can be seen in figure 4.2 that the elastic strain is fully developed at approximately $t = 10^{-3}$. The first datapoint from the simulation is at $t = 0.05$ and to get the same magnitude of the creep strains the zero point where set to the strain value at $t = 1$. The first run of testing different creep parameters can be seen in figure 4.7 where small changes to the creep parameter A of the weave have been tested. The small changes gave only insignificant differences as can be seen when all the simulated lines looks like one in figure 4.7.
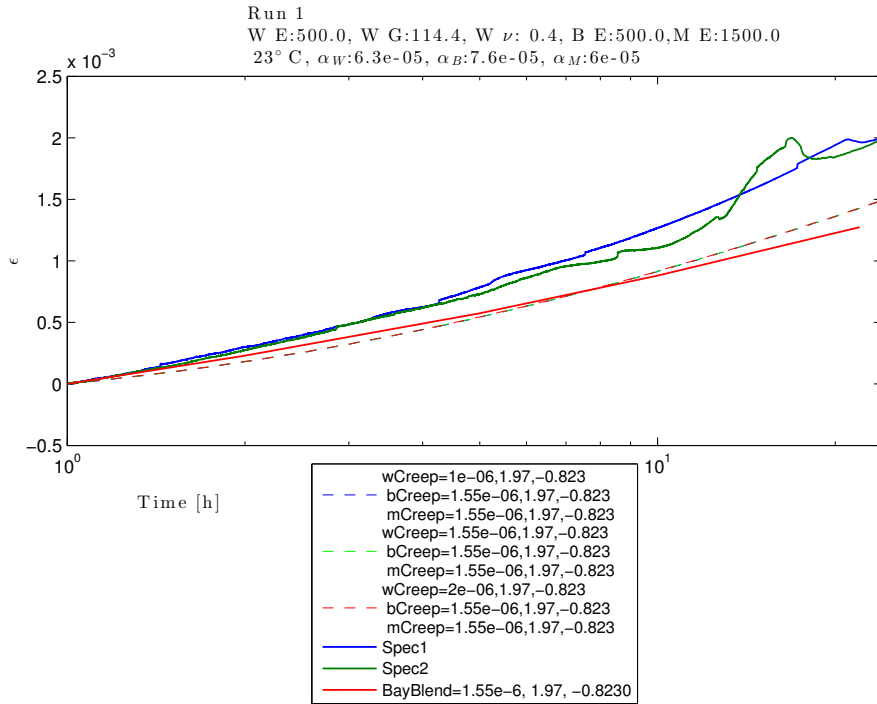
Figure 4.7: *Strains from the experiments, the simulations and the pure Bayblend® T65. The values shifted vertically to have the zero point at $t = 1$ H. wCreep, bCreep and mCreep is the creep parameters for the weave, backing and mix material respectively. The parameters are ordered A, B, n.*

Putting a single number on the correlation is harder in this case because of the time dependency of the creep. An average of the correlation in each time point could express the correlation but the noise in the experimental results would render some numerical difficulties. Therefor the correlation was done using graphs like the one in figure 4.7.

Every simulation done can not be accounted for in this paper but the main findings where that different coefficients of thermal expansion play a very small role in the creep curves. This can be seen in figure 4.8 where the four different combinations of coefficients of thermal expansion for the second set of elasticity parameters at 23° C. The difference between the different parameters are close to non-existing. Hence only one of the sets of thermal coefficients for each of the two sets of elastic parameters where examined and then all were tested when a good correlation was found.
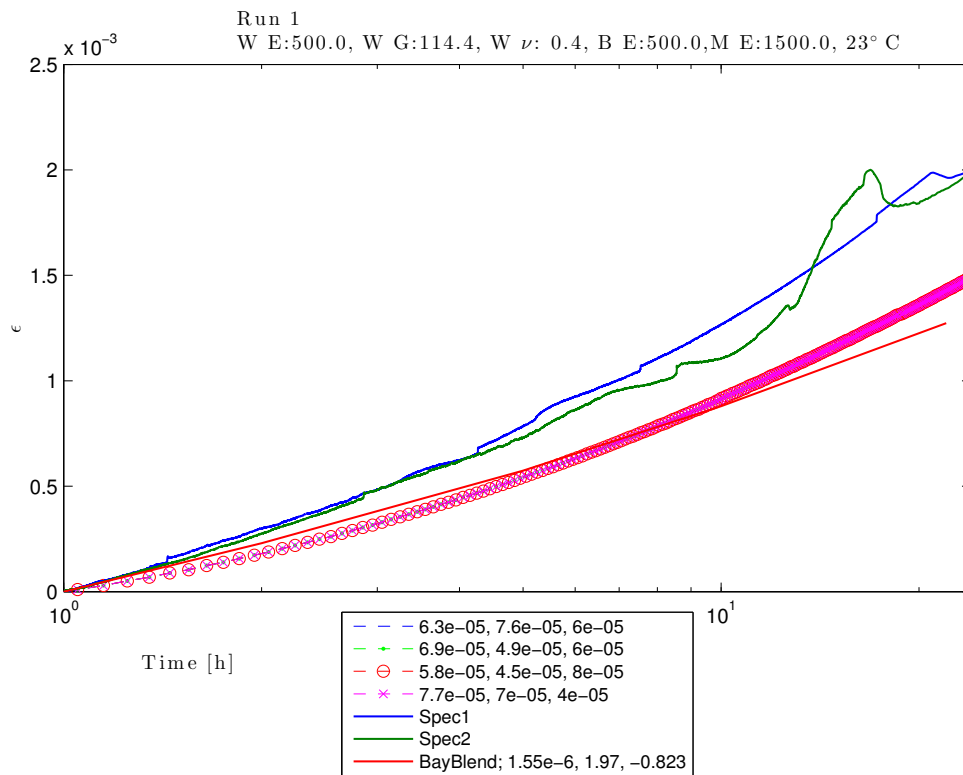
Figure 4.8: *Creep results showing simulations for different combinations of coefficients of thermal expansion. All materials have the same creep parameters as Bayblend® T65*

Trying several different setups the best correlation found for 23° C and the first set of elastic properties can be seen in figure 4.9. The best correlation for the second set of elastic properties can be seen in figure 4.10. The simulations is only for one set of coefficients of thermal expansion but all different tests rendered close to the same result as discussed above.
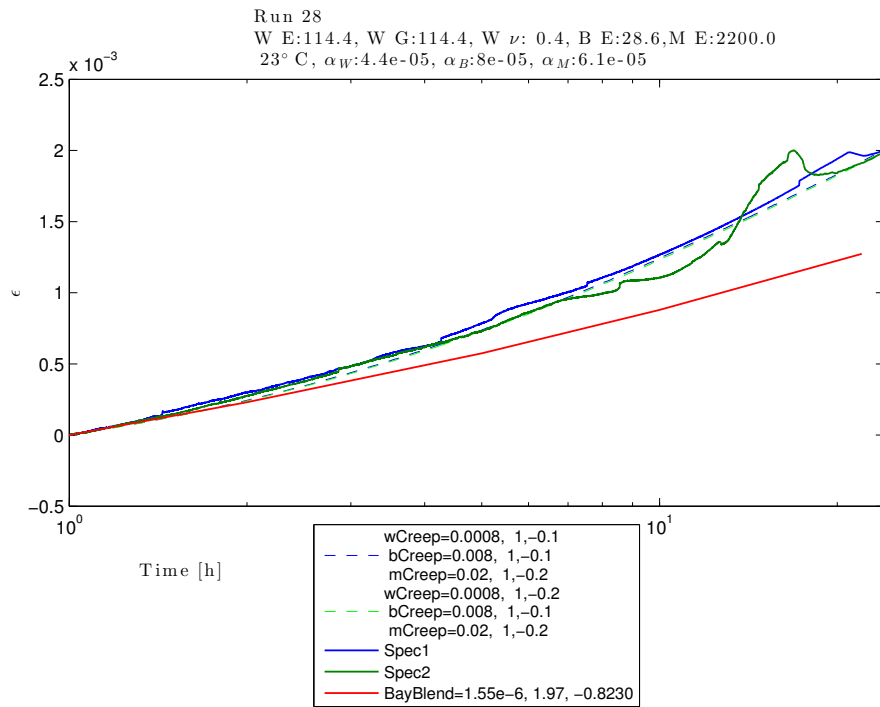
Figure 4.9: *Creep results for the best correlation found at 23° C, first set of elastic properties*
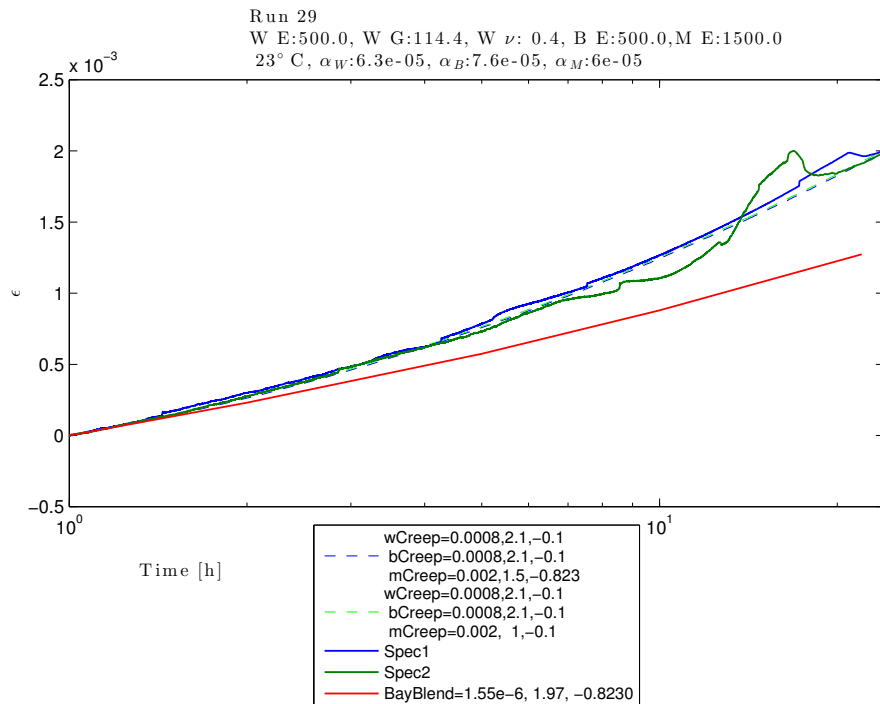
Figure 4.10: *Creep results for the best correlation found at 23° C, second set of elastic properties*

For the 80° C experiment it was hard to find a good correlation. The creep is significantly higher than for a pure Bayblend® T65. Several simulations where conducted but just altering the creep

properties for the weave, backing and mixed layers wasn't enough. Since the boundaries on this thesis were set to treat the Bayblend® T65 as a material with all parameters known it was decided to make an extrapolation of the values found at 23° C using the values of Bayblend® T65 as a base. The correlation of these values can be seen in figure 4.11 and as can be seen it is not good at all.

(a) 1$^{\text{st}}$ set of elastic properties   (b) 2$^{\text{nd}}$ set of elastic properties
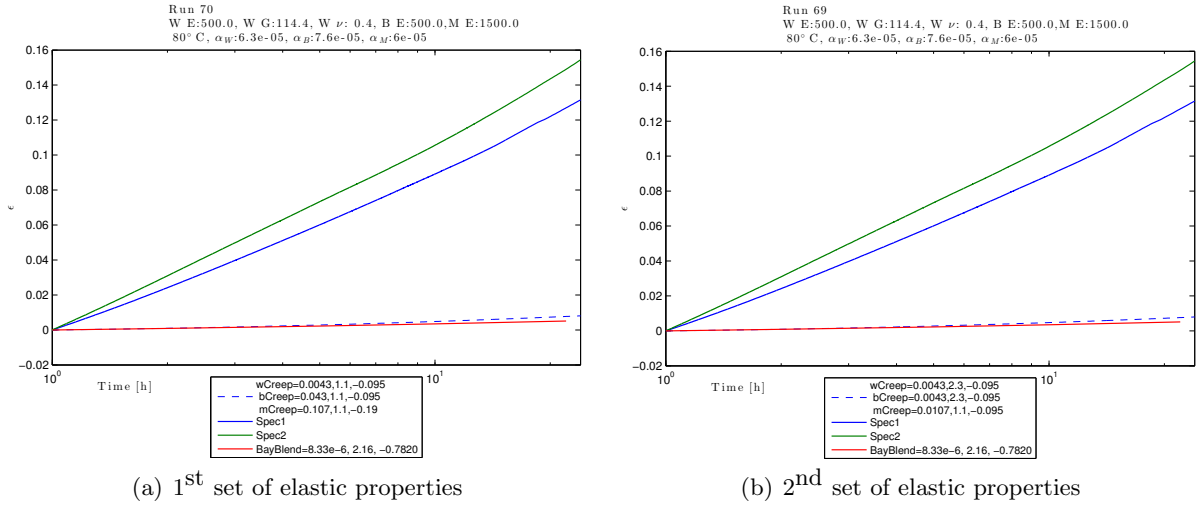
Figure 4.11: *Creep results with creep parameters extrapolated using the Bayblend® T65 as base*

Since this did not give a suitable correlation with the experiment it was also tried to alter the parameters for the creep of Bayblend® T65. For the first set of elastic properties the correlation can be seen in figure 4.12. The second set of elastic properties gave a similar result and the same creep properties will be used. The correlation is not as good as for the 23° C but it will give a interesting comparison on the component level. The different elastic properties that was used in the component simulations can be seen in table 4.5
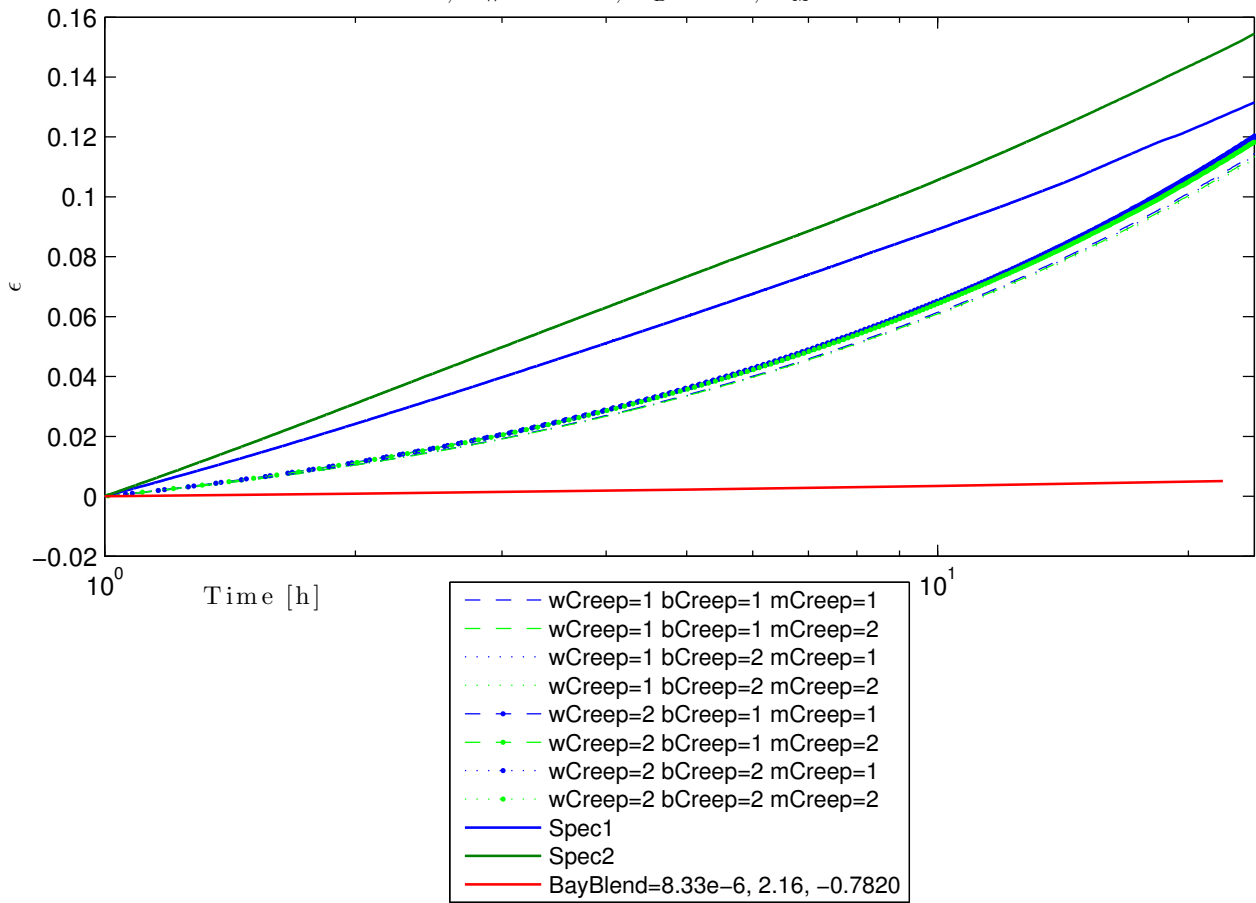
Figure 4.12: *Creep results for the first set of elastic properties where the creep parameters of Bayblend®
T65 is altered*

Table 4.5: Creep parameters used in later simulations

	23° C			80° C		
	A	**B**	**n**	**A**	**B**	**n**
Bayblend® T65 Orig	1.55e-06	1.97	-0.823	8.3300e-06	2.1600	-7.8200e-01
Bayblend® T65 altered	1.55e-06	1.97	-0.823	4.6300e-05	2.5000	-8.0000e-01
Weave elast set 1 Orig	8.00e-04	1.00	-0.1	4.2994e-03	1.0964	-9.5018e-02
Weave elast set 2 Orig	8.00e-04	2.10	-0.1	4.2994e-03	2.3025	-9.5018e-02
Weave elast set 1 altered	8.00e-04	1.00	-0.1	4.6300e-02	3.7100	-5.0000e-01
Weave elast set 2 altered	8.00e-04	2.10	-0.1	4.6300e-02	3.7100	-5.0000e-01
Backing elast set 1 Orig	8.00e-03	1.00	-0.1	4.2994e-02	1.0964	-9.5018e-02
Backing elast set 2 Orig	8.00e-04	2.10	-0.1	4.2994e-03	2.3025	-9.5018e-02
Backing elast set 1 altered	8.00e-03	1.00	-0.1	4.2994e-02	1.0964	-9.5018e-02
Backing elast set 2 altered	8.00e-04	2.10	-0.1	4.2994e-02	1.0964	-9.5018e-02
Mix elast set 1 Orig	2.00e-02	1.00	-0.2	1.0758e-01	1.0964	-1.9004e-01
Mix elast set 2 Orig	2.00e-03	1.00	-0.1	1.0748e-02	1.0964	-9.5018e-02
Mix elast set 1 altered	2.00e-02	1.00	-0.2	1.0748e-01	1.0964	-1.9004e-01
Mix elast set 2 altered	2.00e-03	1.00	-0.1	1.0748e-01	1.0964	-1.9004e-01

4.3 FE-analysis of component

The A-pillar simulation was run using several different material properties but using exactly the same model. The results to compare with is the earlier model which employed the 0.5 mm textile with lower thermal expansion. This results can be seen in figure 4.13. The annotations will be numbered point 1-3 from left to right. In appendix B tables B.1 to B.3 the complete results are presented but there are a couple of points and directions that is especially interesting. These are listed in table 4.6 and are the one that will be discussed.

Table 4.6: Part of the results from the simulation of the component. Rows show the original model, using only Bayblend® T65 and the different thermal sets with original and altered creep properties of Bayblend® T65

Model	displacements [mm]							
	Point 1			**Point 2**		**Point 3**		
	dx	**dz**	**dtot**	**dy**	**dtot**	**dx**	**dz**	**dtot**
Pure plastic	0.66	-0.97	1.18	-0.54	0.55	0.21	0.30	0.36
Original model	0.73	-0.99	1.23	-1.37	1.44	1.48	-1.77	2.33
Therm set=1,orig.B.T65	0.68	-1.33	1.33	-0.34	0.46	-0.32	1.15	1.20
Therm set=4,orig.B.T65	0.68	-1.15	1.33	-0.33	0.46	-0.35	1.19	1.24
Therm set=1,alt.B.T65	0.68	-1.13	1.32	-0.38	0.47	-0.24	1.03	1.06
Therm set=4,alt.B.T65	0.68	-1.14	1.33	-0.35	0.47	-0.31	1.13	1.17

Figure 4.13: *Residual deformations after 800 hours in 85° C when the component is back at room temperature. The original model used earlier where implemented here*

The reason for picking out the directions that are shown in table 4.6 is that they are the once that matter the most. Large deformations in this directions will cause a drop in the perceived quality if the interior trim and are hence most crucial to get right. It can be seen that point 1 gives a fairly good match with the original model but the point 2 gives a smaller deformation. In point 3 the deformation is even in the wrong direction. That the deformations is smaller in point two can be caused by the influence of the curve around the A-pillar. This curve in the geometry influence the

material properties as the fabric is more stretched there and that was not present in the test pieces that the experiments where performed on. In point 1 the fabric is not as stretched since the depth of the mould cavity is smaller there which can explain the better correlation there. In figure 4.14 the results from the first set of thermal properties and the original creep properties of Bayblend® T65 are shown and it can be seen that the deformations is smaller overall which also probably is due to the difference over the geometry that the manufacturing process gives.

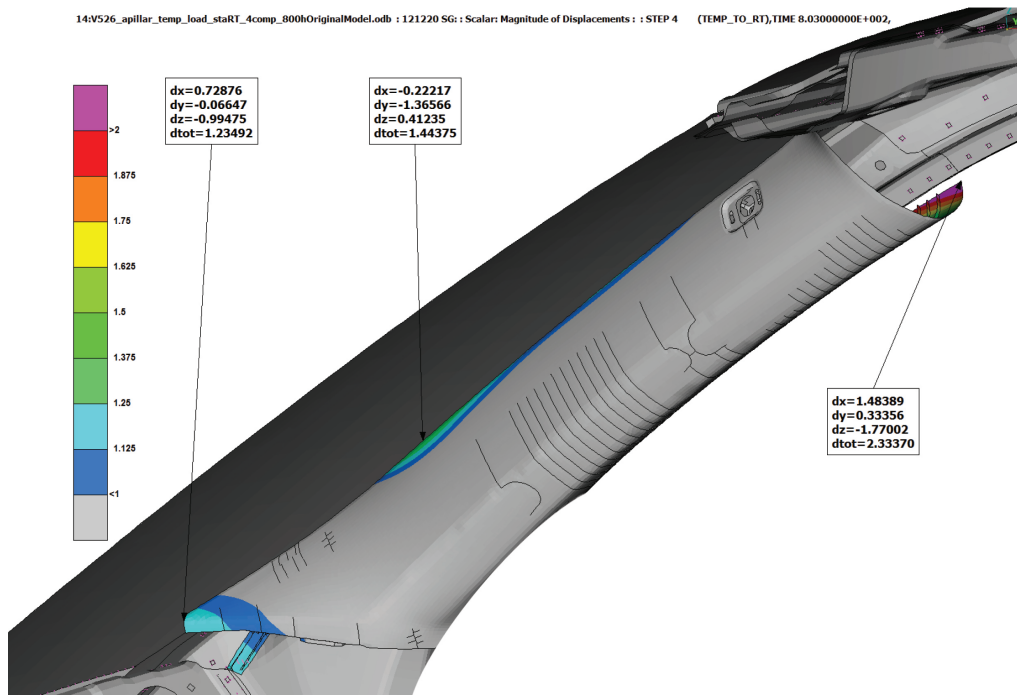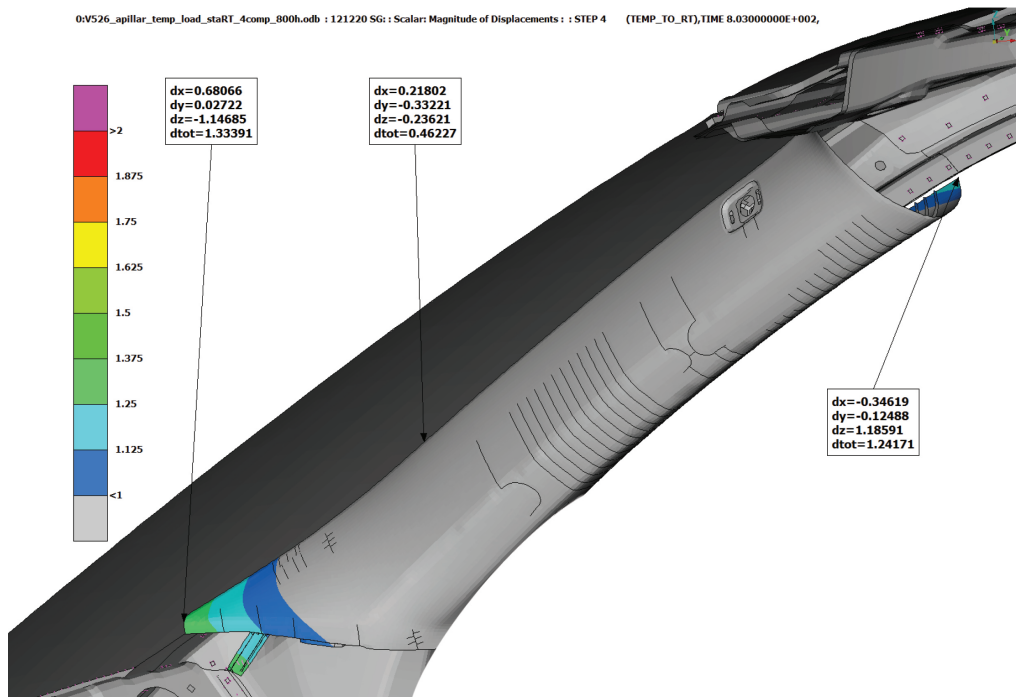**Figure 4.14:** *Residual deformations after 800 hours in 85° C when the component is back at room temperature. The first set of thermal properties where used here with the original creep properties of Bayblend® T65.*

5
Conclusion

T HE PURPOSE OF THIS THESIS was to find a model that could calculate the residual deformations in a fabric upholstered interior trim part after a thermal load. The aim was to get present a generic model which could be updated with new parameters if for instance the textile was changed. Though it has been shown that a four layer composite can be used for this particular combinations of materials changing the textile would require new tests on the material since the textile manufacturer has close to no information about the mechanical properties of their product.

There are several different combinations of parameters for the different plies that gives a good correlation in the coupon tests which is to be expected in this type of correlation. Probably it exists many more combinations that correlates well but as always in engineering the user must decide what is plausible.

The scatter in the experiments is of course a concern. More tests need to be conducted but it is likely that this is the scatter that can be expected. There have been several indications throughout this thesis suggesting that the geometry of a part have a big influence on the solution. The geometry can be crucial in two different ways, first the fabric will stretch differently over the component introducing stresses in the material that vary over the component. This is due to the manufacturing process where a pice of fabric is pushed against the mold by the melt when the cavity is filled. A deeper part of the cavity will of course give a larger stretch in the fabric than a shallow part. Secondly, the geometry influence the results due to the residual stresses in the injected material that is produced by the different cooling speeds in different areas of the component. The textile can also give residual stresses that is unsymmetrical over the thickness due to that the textile insulate the melt and the non-fabric covered side will harden faster than the fabric covered side. These residual stresses can make a component deform considerably in elevated temperatures. Deformations that is very likely to be permanent when the temperature is lowered again.

Reflecting over the questions set up in the beginning of this thesis it can be concluded that some of them have been answered, some where not even relevant and some needs further examination.

It has been shown earlier that the textile does influence the deformations greatly. The initial idea was that the mechanical properties of the textile, especially the thermal elongation, have a big influence but the results in this thesis have shown that it is more likely due to the processes used in the manufacturing. The residual stresses from the manufacturing plays a critical role.

Whether the textile is a viscoelastic material or not is hard to say, probably it is because it is made of a polymer and the experiments showed a significant change between the creep in a pure Bayblend$^{\circledR}$ T65 and the experiments of the fabric upholstered material. The Bayblend$^{\circledR}$ T65 creep parameters were though taken form an earlier experiment and the 80° C experiment showed that it could not only be because of the influence of the textile.

To get an even better understanding about the mechanisms driving the deformations in a fabric upholstered trim panel the manufacturing process needs to be examined since this thesis have shown that the residual stresses from that process plays a key role. A model for predicting the differences over the geometry of a component also needs to be developed since large variations have been found.

Even though this thesis have not given a complete generic model of a textile covered component it is a steppingstone towards getting the knowledge needed to do this kind of simulation with good accuracy.

Bibliography

Agarwal, B. D., Broutman, L. J. and Chandrashekhara, K. (2006). *Analysis and Performance of Fibre Composites*. 3rd ed. Hoboken, USA: Wiley, ISBN: 978-0-471-26891-8.

Bayer MaterialScience (2013). Datasheet Bayblend$^\circledR$ T65 . *Material Data Center*. `http://www.materialdatacenter.com/mb/material/pdf/179732`. (2013-03-01).

Borgstena (2012). Product Specification, Zeus Charcoal Solid PL. Issue: 01. Part no. P72017540401.

Borgstena (2013). Product Specification, Zeus Blond PL. Issue: 03. Part no. P72017540402.

Dassault Systèmes Simulia (2010). Abaqus 6.10 Keywords Reference Manual. *Sharcnet*. `http://www.sharcnet.ca/Software/Abaqus610/Documentation/docs/v6.10/pdf_books/KEYWORD_1.pdf`. (2013-06-27).

Fung, W. (2002). *Coated and Laminated Textiles*. Cambridge: Woodhead Publishing Ltd., ISBN: 1-85573576-8.

Klason, C. and Kubát, J. (2005). *Plaster. Materialval och materialdata.* 5th ed. Lidingö: Industrilitteratr AB, ISBN: 978-9-175-48618-5.

Kuhlmann, G. H. (2001). Manufacuring of Composites Melt Compression Molding (MCM) a One-shot Process for In-mold Lamination and Compression Molding by Melt Strip Deposition. In *Specialized Molding Techniques*, (Heim, H. and Potente, H., eds), pp. 171–185. Wiliam Andrew Inc. Norwich , NY.

Nowacki, W. (1986). *Thermoelasticity.* 2nd ed. Warszawa: Polish Scientific Publishers, ISBN: 0-08-024767-9.

Oldenbo, M. (2009). S80 A-pillar panel sunsim creep. Technical Report 2009-010-01 VCC CAE.

Pötsch, G. and Michaelli, W. (2008). *Injection Moulding: An Introduction.* Second edition. Munich: Hanser, ISBN: 978-3-446-40635-3.

Rabek, J. F. (1996). *Photodegradation of Polymers: Physical Characteristics and Applications.* Heidelberg: Springer-Verlag, ISBN: 978-3-540-60716-8.

Runesson, K., Steinmann, P., Ekh, M. and Menzel, A. (2006). *General Concepts and Inelasticity*, Vol. 1, of *Constitutive modeling of engineering materials - Theory and Computation.*

Volvo Corporate Standard (1994a). Percentage elongation - Textiles. Issue: 02. STD 1024,1127.

Volvo Corporate Standard (1994b). Textiles - woven fabrics - determination of breaking strength and elongation (strip method). Issue: 04. STD 1024,2131.

Volvo Corporate Standard (2005). Tensile stength - Plastics. Issue: 01. STD 1024,1127.

Appendix

Appendix A: Elastic correlation

In this appendix results from the correlation of the tensile experiment and the elastic simulation of the dogbones are presented.

Table A.1: Correlation for different inputs showing the influence of Poisson's ratio ν. W=weave, B=backing and M=mix.

W E_1 **&** E_2	**W** G	**B** E	**M** E	**W** ν	**B** ν	**B** ν	**Corr**	**Diff**
28.6	5.5	15.4	15.4	0.3	0.3	0.3	0.9272	-
28.6	5.5	15.4	15.4	0.4	0.4	0.4	0.9272	0
28.6	5.5	15.4	2200	0.3	0.3	0.3	0.9812	-
28.6	5.5	15.4	2200	0.4	0.4	0.4	0.9806	-6.27e-04
28.6	5.5	500	15.4	0.3	0.3	0.3	0.9392	-
28.6	5.5	500	15.4	0.4	0.4	0.4	0.9392	0
28.6	5.5	500	2200	0.3	0.3	0.3	0.9933	-
28.6	5.5	500	2200	0.4	0.4	0.4	0.9920	-1.28e-03
500	500	15.4	15.4	0.3	0.3	0.3	1.0083	-
500	500	15.4	15.4	0.4	0.4	0.4	1.0116	3.33e-03
500	500	15.4	2200	0.3	0.3	0.3	1.0619	-
500	500	15.4	2200	0.4	0.4	0.4	1.0651	3.22e-03
500	500	500	15.4	0.3	0.3	0.3	1.0204	-
500	500	500	15.4	0.4	0.4	0.4	1.0231	2.72e-03
500	500	500	2200	0.3	0.3	0.3	1.0745	-
500	500	500	2200	0.4	0.4	0.4	1.0770	2.54e-03

Table A.2: Correlation for different input values of the Young's modulus for the different materials, W=weave, B=backing and M=mix. Poisson's ratio was set to 0.4 for all materials. The rightmost column, called Diff, is the difference from perfect correlation. The bold values are the ones chosen for further investigation.

M E	**B** E	**W** E_1 **&** E_2	**W** G	**Corr**	**Diff**
1500	28.6	500	114.4	9.93e-01	7.36e-03
1500	57.2	500	114.4	9.94e-01	6.07e-03
1500	114.4	114.4	114.4	9.85e-01	1.50e-02
1500	114.4	500	114.4	9.95e-01	5.42e-03
1500	500	114.4	114.4	9.94e-01	6.07e-03
1500	**500**	**500**	**114.4**	**1.00e+00**	**3.69e-03**
2200	15.4	28.6	57.2	9.89e-01	1.12e-02
2200	15.4	57.2	57.2	9.89e-01	1.06e-02
2200	15.4	57.2	114.4	9.98e-01	2.19e-03
2200	28.6	28.6	57.2	9.89e-01	1.06e-02
2200	28.6	57.2	28.6	9.85e-01	1.50e-02
2200	28.6	57.2	57.2	9.90e-01	9.92e-03
2200	28.6	57.2	114.4	9.98e-01	1.54e-03
2200	28.6	114.4	57.2	9.91e-01	8.64e-03
2200	**28.6**	**114.4**	**114.4**	**1.00e+00**	**2.37e-04**
2200	28.6	500	114.4	1.01e+00	1.03e-02
2200	57.2	28.6	28.6	9.85e-01	1.50e-02
2200	57.2	28.6	57.2	9.89e-01	1.06e-02
2200	57.2	57.2	28.6	9.86e-01	1.44e-02
2200	57.2	57.2	57.2	9.90e-01	9.92e-03
2200	57.2	57.2	114.4	9.99e-01	8.88e-04
2200	57.2	114.4	57.2	9.92e-01	8.00e-03
2200	57.2	114.4	114.4	1.00e+00	4.15e-04
2200	57.2	500	114.4	1.01e+00	1.03e-02
2200	114.4	28.6	57.2	9.91e-01	9.28e-03
2200	114.4	57.2	114.4	1.00e+00	4.15e-04
2200	114.4	114.4	57.2	9.93e-01	6.71e-03
2200	114.4	114.4	114.4	1.00e+00	1.72e-03
2200	114.4	500	114.4	1.01e+00	1.23e-02
2200	500	114.4	114.4	1.01e+00	1.10e-02

Appendix B: Deformations on component level

This appendix include the complete results for the three points in the deformation analysis discussed in section 4.3.

Table B.1: Deformations in point 1 on the component level for different sets of material data. Using both the altered and the original Bayblend® T65 creep properties.

	dx	dy	dz	dtot
Pure plastic	0.66113	-0.00787	-0.97485	1.17792
Original model	0.72876	-0.06647	-0.99475	1.23492
Therm set=1,orig.B.T65	0.68140	0.02618	-1.32650	1.32650
Therm set=2,orig.B.T65	0.67969	0.02625	-1.13733	1.32521
Therm set=3,orig.B.T65	0.67944	0.02631	-1.13721	1.32498
Therm set=4,orig.B.T65	0.68066	0.02722	-1.14685	1.33391
Therm set=5,orig.B.T65	0.67847	0.02722	-1.14661	1.33258
Therm set=6,orig.B.T65	0.68628	0.02710	-1.14917	1.33877
Therm set=7, orig.B.T65	0.67163	0.02710	-1.14417	1.32700
Therm set=1,alt.B.T65	0.68384	0.92240	-1.13159	1.32236
Therm set=2,alt.B.T65	0.68066	0.02258	-1.12695	1.31675
Therm set=3,alt.B.T65	0.67969	0.02264	-1.12585	1.31531
Therm set=4,alt.B.T65	0.68042	0.02533	-1.14331	1.33070
Therm set=5,alt.B.T65	0.67725	0.02502	-1.14026	1.32645
Therm set=6,alt.B.T65	0.68628	0.02521	-1.14661	1.33653
Therm set=7,alt.B.T65	0.66650	0.02374	-1.12805	1.31045

Table B.2: Deformations in point 2 on the component level for different sets of material data. Using both the altered and the original Bayblend® T65 creep properties.

	dx	**dy**	**dz**	**dtot**
Pure plastic	0.11670	-0.53839	-0.05884	0.55403
Original model	-0.22217	-1.36566	0.41235	1.44375
Therm set=1,orig.B.T65	0.21436	-0.33911	-0.23047	0.46267
Therm set=2,orig.B.T65	0.21411	-0.33752	-0.23083	0.46157
Therm set=3,orig.B.T65	0.21411	-0.33698	-0.23096	0.46123
Therm set=4,orig.B.T65	0.21802	-0.33221	-0.23621	0.46227
Therm set=5,orig.B.T65	0.21704	-0.33142	-0.23596	0.46111
Therm set=6,orig.B.T65	0.21899	-0.33734	-0.23535	0.46599
Therm set=7, orig.B.T65	0.21655	-0.32428	-0.23816	0.45692
Therm set=1,alt.B.T65	0.19849	-0.37604	-0.20642	0.47266
Therm set=2,alt.B.T65	0.19995	-0.36957	-0.20776	0.46875
Therm set=3,alt.B.T65	0.20020	-0.36768	-0.20837	0.46764
Therm set=4,alt.B.T65	0.20898	-0.34943	-0.22498	0.46517
Therm set=5,alt.B.T65	0.20898	-0.34595	-0.22559	0.46286
Therm set=6,alt.B.T65	0.20996	-0.35421	-0.22485	0.46923
Therm set=7,alt.B.T65	0.21338	-0.32581	-0.23254	0.45360

Table B.3: Deformations in point 3 on the component level for different sets of material data. Using both the altered and the original Bayblend® T65 creep properties.

	dx	dy	dz	dtot
Pure plastic	0.21216	0.01178	0.29602	0.36439
Original model	1.48389	0.33356	-1.77002	2.33370
Therm set=1,orig.B.T65	-0.32471	-0.12311	1.15381	1.20493
Therm set=2,orig.B.T65	-0.32544	-0.12433	1.15576	1.20713
Therm set=3,orig.B.T65	-0.32617	-0.12463	1.15686	1.20841
Therm set=4,orig.B.T65	-0.34619	-0.12488	1.18591	1.24171
Therm set=5,orig.B.T65	-0.34497	-0.12543	1.18542	1.24095
Therm set=6,orig.B.T65	-0.34424	-0.12238	1.17969	1.23496
Therm set=7, orig.B.T65	-0.31156	-0.12671	1.19897	1.25586
Therm set=1,alt.B.T65	-0.24072	-0.10748	1.02612	1.05945
Therm set=2,alt.B.T65	-0.24634	-0.10950	1.03491	1.06945
Therm set=3,alt.B.T65	-0.24878	-0.10986	1.03845	1.07347
Therm set=4,alt.B.T65	-0.30786	-0.12000	1.12549	1.17299
Therm set=5,alt.B.T65	-0.31128	-0.11841	1.13208	1.18005
Therm set=6,alt.B.T65	-0.30713	-0.11853	1.12146	1.16878
Therm set=7,alt.B.T65	-0.33789	-0.10968	1.17432	1.22687